THE JOURNAL OF PHYSICAL CHEMISTRY C

Article

pubs.acs.org/JPCC

# A ReaxFF Investigation of Hydride Formation in Palladium Nanoclusters via Monte Carlo and Molecular Dynamics Simulations

Thomas P. Senftle,[†] Michael J. Janik,*[,†] and Adri C. T. van Duin*[,‡]

[†]Department of Chemical Engineering, Pennsylvania State University, University Park, Pennsylvania 16802, United States

[‡]Department of Mechanical and Nuclear Engineering, Pennsylvania State University, University Park, Pennsylvania 16802, United States

Supporting Information

**ABSTRACT:** Palladium can readily dissociate and absorb hydrogen from the gas phase, making it applicable in hydrogen storage devices, separation membranes, and hydrogenation catalysts. To investigate hydrogen transport properties in Pd on the atomic scale, we derived a ReaxFF interaction potential for Pd/H from an extensive set of quantum data for both bulk and surface properties. Using this potential, we employed a recently developed hybrid grand canonical-Monte Carlo/molecular dynamics (GC-MC/MD) method to derive theoretical hydrogen absorption isotherms in Pd bulk crystals and nanoclusters for hydrogen pressures ranging from $10^{-1}$ atm to $10^{-14}$ atm, and at temperatures ranging from 300 to 500 K. Analysis of the equilibrated cluster structures reveals the contributing roles of surface, subsurface, and bulk regions during the size-dependent transition between the solid solution $\alpha$ phase and the hydride $\beta$ phase. Additionally, MD simulations of the dissociative adsorption of hydrogen from the gas phase were conducted to assess size-dependent kinetics of hydride formation in Pd clusters. Hydrogen diffusion coefficients, apparent diffusion barriers, and pre-exponential factors were derived from MD simulations of hydrogen diffusion in bulk Pd. Both the thermodynamic results of the GC-MC/MD method and the kinetic results of the MD simulations are in agreement with experimental values reported in the literature, thus validating the Pd/H interaction potential, and demonstrating the capability of the GC−MC and MD methods for modeling the complex and dynamic phase behavior of hydrogen in Pd bulk and clusters.

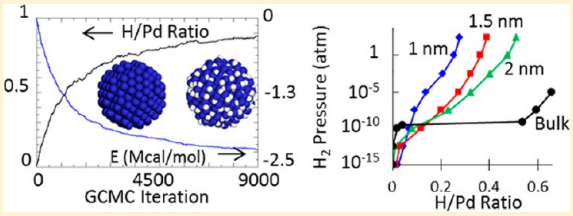


## 1. INTRODUCTION

Palladium can dissociate and absorb hydrogen from the gas phase, making it an extensively studied medium for application in hydrogen storage devices,[1−4] hydrogen separation membranes,[5−7] and hydrogenation catalysts.[8−13] Hydrogen can be incorporated in bulk palladium in two distinct $PdH_x$ phases, called the "$\alpha$" phase and the "$\beta$" phase, which differ in hydrogen concentration.[14] At low hydrogen concentrations ($\sim x < 0.1$), the $\alpha$ phase consists of a solid solution in which hydrogen atoms occupy random interstitial octahedral sites in the fcc lattice of palladium. As the hydrogen concentration increases ($\sim x > 0.6$), a transition to the $\beta$ phase occurs, marked by an increase in the fcc lattice constant. The structures of the solid solution $\alpha$ phase and the hydride $\beta$ phase only differ by the hydrogen concentration and the fcc lattice constant. This phase change displays a characteristic plateau on a pressure−composition isotherm caused by the miscibility gap (MG) separating the low concentration $\alpha$ phase and the high concentration $\beta$ phase. The extent of the MG and its location on the pressure−composition isotherm, namely, its dependence on temperature and pressure, varies between bulk and cluster systems, and is additionally affected by cluster size[15−17] and preparation method.[18] The effects of temperature, pressure, cluster size, and preparation method must be understood to optimize the design of Pd-based processes for hydrogen separation, storage, and catalysis.

Hydrogen sorption by Pd surfaces, clusters, and bulk has been investigated extensively in numerous experimental and theoretical studies.[19−36] Compared to the bulk, Pd clusters display a narrower MG characterized by an increased maximum hydrogen concentration in the $\alpha$ phase, a decreased minimum concentration in the $\beta$ phase, and an increased slope in the isotherm-plateau connecting the phases. The MG continually narrows with decreasing cluster size,[37−39] and in some cases closes completely,[15,16] indicating that there may be a critical cluster size below which the phase change does not occur. Using X-ray diffraction (XRD), Pundt and co-workers[15] found that the phase transition occurs in 6.0 nm clusters and does not occur in 3.8 nm clusters, where both clusters were stabilized by a surfactant shell. Similarly, Konopsky et al.[16] demonstrated by observing photonic crystal surface waves (PC SWs) that, when supported on $Ta_2O_5/SiO_2$, the phase transition occurs in 6.0 nm clusters and does not occur in 2.0 nm clusters.

The existence of the MG in small clusters and the impact of surface stabilizers or supports remains an open question. Ingham et al.[17] measured lattice expansions via in situ XRD and found that the MG remains open for naked 6.1 nm, 3.0 nm, and 1.7 nm clusters supported on a weakly interacting $Si/SiO_2$

**Received:** November 8, 2013
**Revised:** February 5, 2014
**Published:** February 11, 2014

substrate. They contend that the increased solubility of the $\alpha$ phase, and thus the narrowing of the MG, is the result of surface interactions affecting the hydrogen absorption capability of the underlying bulk-like core region of the cluster, and that the nature of the surfactant, polymer, or support used to stabilize the cluster alters these surface interactions; this explains why the MG closes in studies conducted on small clusters with strongly interacting stabilizers. The impact of the cluster stabilizer is further demonstrated by Suleiman et al.,[18] who found that the MG in polymer stabilized clusters occurs over a wider pressure range than in the analogous surfactant stabilized clusters, which is related to differing mechanical stain imparted on the cluster lattice by the stabilizers. Additionally, Wilde et al.[40] utilized a nuclear reaction analysis (NRA) technique to differentiate between hydrogen uptake in surface, subsurface, and bulk sites, showing that the increased solubility of the $\alpha$ phase consists of H atoms absorbed in the cluster's bulk-like core volume. This demonstrates that the narrowing of the MG in clusters cannot be attributed solely to additional surface and subsurface sites available in clusters compared to the bulk, as had been previously proposed.[37,41]

These results, among numerous others, demonstrate the complex nature of hydride formation in Pd clusters, and underscore the necessity of an atomic level understanding of the hydride formation process. Herein, we describe the development of an empirical reactive force-field, using the ReaxFF formalism,[42] for Pd/H. We have employed this potential in grand canonical Monte Carlo (GC-MC) simulations to derive theoretical hydrogen absorption isotherms in Pd bulk and clusters (sizes ranging from 1.0 to 2.0 nm), and have analyzed the resulting structural properties to assess the role of surface, subsurface, and bulk hydrogen adsorption sites. Additionally, we have conducted molecular dynamics simulations to investigate the initial kinetics of hydrogen uptake from the gas phase by Pd clusters, and the concentration dependence of hydrogen diffusion in bulk Pd. Together, these simulations enable us to assess both the thermodynamic and kinetic properties of hydride formation in palladium on the atomic scale. Furthermore, the Pd/H parameters developed here are fully transferable with previously developed Pd/O parameters,[43] making the future extension to Pd/O/H and Pd/C/O/H descriptions straightforward. Such descriptions will be instrumental in ReaxFF studies of hydrocarbon oxidation, hydrogenation, and combustion over Pd-based catalysts.

## 2. THEORY AND METHODS

**2.1. ReaxFF Potential.** Empirical force-field methods, such as ReaxFF, are computationally inexpensive compared to direct quantum methods, enabling studies to reach larger length and time scales. These methods can help bridge the size gap between macroscopic experimental investigations and studies utilizing quantum calculations. The ReaxFF potential[42] is a reactive force field comprised of bond-order/bond-length relationships[44,45] combined with polarizable charge descriptions[46] to describe covalent, Coulomb, and van der Waals interactions between atoms in a system. It was originally developed to treat hydrocarbon systems,[42,47] and has been extended to model multiphase interfaces,[48−50] including dissociative $H_2$ adsorption on Pt[51] and Fe.[52] ReaxFF is well suited for investigations of hydride formation in Pd, as the Pd/H parameters developed here are transferable between gas and surface species, allowing the potential to model hydrogen dissociation and absorption across the gas/surface interface.

The details of the ReaxFF potential have been described previously,[42] and are only briefly restated here. Covalent terms in the interaction potential, such as bond-energy, three-body valence angle strain, and four-body torsion angle strain, are calculated as an explicit function of bond order, which is in turn calculated from interatomic distance using the equation:

$$\mathrm{BO}_{ij} = \mathrm{BO}_{ij}^{\sigma} + \mathrm{BO}_{ij}^{\pi} + \mathrm{BO}_{ij}^{\pi\pi} = \exp\left[p_{\mathrm{bo1}}\left(\frac{r_{ij}}{r_{\mathrm{o}}^{\sigma}}\right)^{p_{\mathrm{bo2}}}\right] + \exp\left[p_{\mathrm{bo3}}\left(\frac{r_{ij}}{r_{\mathrm{o}}^{\pi}}\right)^{p_{\mathrm{bo4}}}\right] + \exp\left[p_{\mathrm{bo5}}\left(\frac{r_{ij}}{r_{\mathrm{o}}^{\pi\pi}}\right)^{p_{\mathrm{bo6}}}\right] \quad (1)$$

where $\mathrm{BO}_{ij}$ is the bond-order between atoms $i$ and $j$, $r_{ij}$ is interatomic distance, $r_{\mathrm{o}}$ terms are equilibrium bond lengths, and $p_{\mathrm{bo}}$ terms are empirical parameters fit to experimental or quantum data. This bond-length/bond-order formalism produces smooth transitions between $\sigma$, $\pi$, and $\pi\pi$ bond character, and can thus be used in simulations involving bond dissociation and formation during reactive events. Additionally, electrostatic and dispersive interactions are calculated between all atom pairs from interatomic distances, regardless of bond-order. Electrostatic interactions are treated with a self-consistent electron equilibration method (EEM). This method determines atomic partial charges from the system configuration; the partial charges are then employed in a shielded Coulombic potential.[46] In this study, the ReaxFF parameters unique to Pd/H interactions were derived using a previously developed single-parameter optimization scheme,[53] which minimizes deviation between ReaxFF and quantum data in a training set populated with bulk, surface, and gas phase data for palladium and hydrogen. The contents of this training set and the parameter optimization process are described in Section 3.1.

**2.2. Monte Carlo Method.** We implement a recently developed[43] hybrid grand canonical Monte Carlo/molecular dynamics (GC-MC/MD) method to investigate hydrogen absorption in Pd clusters and bulk. For cluster simulations, the GC-MC/MD method is employed in a $TV\mu_{\mathrm{H2}}N_{\mathrm{Pd}}$ ensemble with constant temperature ($T$), volume ($V$), hydrogen chemical potential ($\mu_{\mathrm{H2}}$), and number of Pd atoms ($N_{\mathrm{Pd}}$). Cluster simulations do not require a variable system volume because the cluster can expand into a surrounding vacuum space to accommodate absorbed hydrogen atoms in the metal lattice, which is not possible in periodic bulk simulations. For periodic bulk simulations, a $TP\mu_{\mathrm{H2}}N_{\mathrm{Pd}}$ ensemble, with constant pressure and variable volume, is required to allow for lattice expansion upon hydrogen uptake. Hence, we have extended the previously reported GC-MC/MD method to include stochastic volume changes in a fixed pressure ensemble, similar to the GC-MC methods employed to investigate Pd/H systems by Ray and co-workers[54,55] and by Debiaggi and co-workers.[56−58] The following MC moves are available in the $TV\mu_{\mathrm{H2}}N_{\mathrm{Pd}}$ ensemble: (1) insertion of a hydrogen atom into the system at a random position, (2) deletion of a randomly selected hydrogen atom from the system, or (3) displacement of a hydrogen atom to a new random position in the system. The same MC moves are available in the $TP\mu_{\mathrm{H2}}N_{\mathrm{Pd}}$ ensemble, with the addition of a volume-change MC move that allows the system volume to cubically expand or contract by a randomly selected amount.


dx.doi.org/10.1021/jp411015a | J. Phys. Chem. C 2014, 118, 4967−4981

**Table 1. ReaxFF Parameters for Pd/H Interactions**

| atom | $r_o$ | $\eta$ | $\chi$ | $\gamma$ | $r_{vdW}$ | $\epsilon_{vdW}$ | $\alpha$ | $\gamma_{vdW}$ | $p_{ov/un}$ |
|---|---|---|---|---|---|---|---|---|---|
| Pd[a] | 1.8582 | 6.6477 | 5.5005 | 1.0000 | 2.0113 | 0.2465 | 12.5712 | 6.0083 | −13.0000 |
| H[b] | 0.8930 | 9.6093 | 3.7248 | 0.8203 | 1.3550 | 0.0930 | 8.2230 | 33.2894 | −19.4571 |

| bond | $D_e^\sigma$ | $p_{be,1}$ | $p_{cov}$ | $p_{be,2}$ | $p_{bo,1}$ | $p_{bo,2}$ |
|---|---|---|---|---|---|---|
| Pd−Pd[a] | 90.7003 | −0.1661 | 0.2578 | 3.0618 | −0.0914 | 5.4665 |
| H−H[b] | 153.3934 | −0.4600 | 0.7300 | 6.2500 | −0.0790 | 6.0552 |
| Pd−H[c] | 67.5406 | 0.6327 | 0.2077 | 0.7493 | −0.0547 | 4.0000 |

| off-diagonal | $r^\sigma$ | $R_{vdW}$ | $\gamma$ | $\epsilon^\sigma$ |
|---|---|---|---|---|
| Pd−H | 1.5714 | 1.1103 | 13.0000 | 0.1445 |

| angle | $\theta_o$ | $k_a$ | $k_b$ | $p_{val,1}$ | $p_{val,2}$ |
|---|---|---|---|---|---|
| Pd−Pd−H | 40.0354 | 9.2882 | 8.0000 | 1.0000 | 2.7288 |
| Pd−H−Pd | 0.9367 | 12.0943 | 6.6344 | 1.0000 | 1.0115 |
| H−Pd−H | 25.6680 | 10.1984 | 7.6844 | 1.0000 | 1.2474 |
| Pd−H−H | 83.9156 | 13.0474 | 0.9983 | 1.0000 | 3.1381 |

[a]Palladium atom parameters from ref 43. [b]Hydrogen parameters from ref 50. [c]Units: $r$ terms in Å; $\gamma$ terms in Å$^{-1}$; $\epsilon$, $D$, and $k_a$ terms in kcal mol$^{-1}$; $\eta$ and $\chi$ in eV; $\theta_o$ in degrees; $k_b$ in (1/radians)$^2$; all other terms are dimensionless.

The following acceptance criteria, derived from detail-balance Boltzmann relationships,[59,60] were applied for atom insertion, deletion, displacement, or volume-change moves during a Monte Carlo step:

$$P_{insert}^{accept} = \min\left[1, \frac{V}{\Lambda^3(N+1)} \exp[-\beta(E_2 - E_1 - \mu_{res})]\right] \quad (2)$$

$$P_{delete}^{accept} = \min\left[1, \frac{N\Lambda^3}{V} \exp[-\beta(E_2 - E_1 + \mu_{res})]\right] \quad (3)$$

$$P_{displace}^{accept} = \min[1, \exp[-\beta(E_2 - E_1)]] \quad (4)$$

$$P_{volume}^{accept} = \min\left[1, \exp\left[-\beta\left((E_2 - E_1) + P(V_2 - V_1) - Nk_bT \ln\left(\frac{V_2}{V_1}\right)\right)\right]\right] \quad (5)$$

where $N$ is the number of exchangeable atoms in the system before the MC move, $\Lambda$ is the thermal de Broglie wavelength of the exchanged atom, $\beta$ is the Boltzmann factor given by $\beta = 1/(k_bT)$, $E_1$ and $E_2$ are the potential energies calculated as a function of atom configurations in the system before and after the MC move, $V_1$ and $V_2$ are the system volumes before and after a volume-change MC move, $P$ is pressure, and $\mu_{res}$ is the chemical potential of the hydrogen reservoir. The gas phase pressures considered here are on the order of ∼1 atm and are not large enough to significantly affect the bulk system volume through mechanical stress, and thus the $PV$ term in eq 5 is negligible. In this study, $\mu_{res}$ for hydrogen is related to $T$ and $P$ by the following equation:

$$\mu_{res}(T, P) = \frac{1}{2}\left[\mu_{H_2}(T, P^o) + k_bT \ln\left(\frac{P}{P^o}\right) - E_d\right] \quad (6)$$

where $\mu_{H2}(T,P^o)$ is the experimentally determined chemical potential of $H_2$ at $T$ and $P^o$ available from published thermodynamic tables,[61] and $E_d$ is the zero-Kelvin bond dissociation energy of $H_2$. Since the Pd/H ReaxFF parameters were derived from DFT-PW91 values for hydrogen adsorption energies that were calculated relative to gas phase $H_2$, the DFT-PW91 $H_2$ dissociation energy of 105.1 kcal mol$^{-1}$ was used for $E_d$ to remain consistent with the DFT values used for ReaxFF training. We note that the PW91 functional used here yields values for hydrogen binding that are typically higher than those observed experimentally,[20,21,32,35] which will shift palladium hydride phase boundaries predicted by our GC-MC/MD method to lower hydrogen pressures. This systematic error does not affect qualitative conclusions drawn from the results presented herein, but must be taken into account for quantitative comparisons to experimental values. The relative extent and impact of this deviation is discussed in detail in Section 3 where appropriate.

As discussed in a previous publication,[43] the GC-MC/MD method introduces a MD-based energy minimization step after each MC trial move to allow a structural relaxation in the system prior to applying the acceptance criteria in eqs 2−5. This additional step reduces the number of MC iterations required to reach equilibrium compared to pure GC-MC simulations; the energy minimization step prevents hydrogen atoms from being placed in high-energy locations occupied by metal atoms, thus increasing MC acceptance rates. Here, we employ a conjugate gradient (CG) relaxation of forces, with a convergence criterion of 0.5 kcal mol$^{-1}$ between subsequent CG steps. The 0.5 kcal mol$^{-1}$ convergence criteria was selected because it is tight enough to prevent inserted H atoms from being placed within the atomic radius of any Pd atom, and is loose enough to converge in a reasonable time frame. Tighter and looser convergence criteria impact the computational time required for the MC run to reach equilibrium, but do not significantly impact the final equilibrium values.

**2.3. Quantum Method.** The Vienna ab initio simulation package (VASP) was employed for all density functional theory (DFT) calculations.[62,63] The generalized gradient approximation (GGA) was used to treat the exchange-correlation functional, as implemented by the Perdew−Wang formulation (PW91).[64] Plane-wave basis sets were employed in all calculations, and were truncated at 450 eV for periodic surface calculations and 725 eV for bulk calculations. The atomic force convergence criterion for all structural optimizations was 0.05 eV Å$^{-1}$. The projector augmented wave method[65] (PAW) was employed to represent core electron regions with valence configurations of 4d$^{10}$ for Pd atoms and 1s$^1$ for H atoms. The Monkhorst-Pack[66] (MP) Brillouin zone sampling method was


dx.doi.org/10.1021/jp411015a | J. Phys. Chem. C 2014, 118, 4967−4981

utilized for periodic calculations. Pd surface calculations used a 3 × 3 × 1 MP k-point spacing in a four-layer 3 × 3 periodic cell with a 20 Å vacuum layer separating images perpendicular to the surface. The bottom two Pd layers were fixed during structural optimizations, while the top two surface layers were allowed to relax. A 7 × 7 × 7 MP k-point spacing was used for bulk $PdH_x$ calculations with a 2 × 2 × 2 fcc lattice in a triclinic $\alpha = \beta = \gamma = 60°$ unit cell (containing 8 Pd atoms, and $x = 1$ to $x = 8$ H atoms). Cluster and molecule calculations were conducted in a 45 Å × 45 Å × 45 Å periodic box, in which the Γ point was considered. The climbing image nudged elastic band (CI-NEB) method[67] was used to identify transition states for hydrogen migration.

## 3. RESULTS AND DISCUSSION

**3.1. Pd/H Force-Field Development.** A DFT training set consisting of bulk formation energies, surface adsorption energies, and transition state barriers was used to optimize the Pd/H interaction parameters shown in Table 1. These parameters were used in conjunction with previously published Pd/Pd[43] and H/H[50] interaction parameters, which are also provided in Table 1. The ReaxFF general parameters and the entire Pd/H parameter set are provided in ReaxFF input format in the Supporting Information. Again, the Pd/H parameters provided here are fully transferable with the previous Pd/O parameter set,[43] which will allow for the direct extension to a Pd/O/H description.

*Bulk Hydride.* The ReaxFF potential was trained to reproduce hydrogen adsorption behavior in bulk palladium. Palladium readily forms two phases upon exposure to hydrogen: a low concentration $\alpha$ phase and a high-concentration $\beta$ phase. Both phases consist of H atoms absorbed interstitially in Pd fcc-octahedral sites, and vary only in concentration and fcc lattice parameter. The Pd/H interaction parameters were trained to correctly reproduce bulk properties related to this phase behavior. The potential was trained to reproduce lattice expansion upon hydride formation by fitting against a DFT energy-volume curve for two stoichiometric PdH structures, shown in Figure 1. One is the energetically favored NaCl-type structure, in which H atoms occupy octahedral sites in a fcc Pd lattice. The other is a simple cubic structure, where a single H atom is placed in the center of a cubic Pd unit cell. Although the cubic structure is high in energy and is not experimentally realizable, it is included to diversify the ReaxFF training set to ensure that the potential does not improperly favor such high energy structures. For the NaCl-type structure, ReaxFF predicts an equilibrium lattice spacing of 4.24 Å and a corresponding formation energy of −2.56 kcal $mol^{-1}$, compared to our DFT values of 4.15 Å and −3.04 kcal $mol^{-1}$ and the DFT values reported by Grönbeck and Zhdanov[34] of 4.11 Å and −5.3 kcal $mol^{-1}$. The equilibrium lattice spacing predicted by DFT for the high concentration $\beta$ phase is longer than the experimental[17,31] value of ∼4.02 Å. This variation can be attributed to the PW91 functional, which yields an elongated Pd fcc lattice spacing of 3.97 Å compared to the experimental[68] value of 3.89 Å. To account for phase behavior arising from varying hydrogen concentrations, the potential was additionally optimized against DFT formation energies for bulk $PdH_x$ with $x$ ranging from 0.125 to 1.0, where the formation energy is calculated relative to gas phase $H_2$ and a $PdH_0$ bulk where all H atoms have been removed (i.e., an expanded Pd-fcc lattice). The results, shown in Figure 2, demonstrate good agreement between ReaxFF and DFT. Both

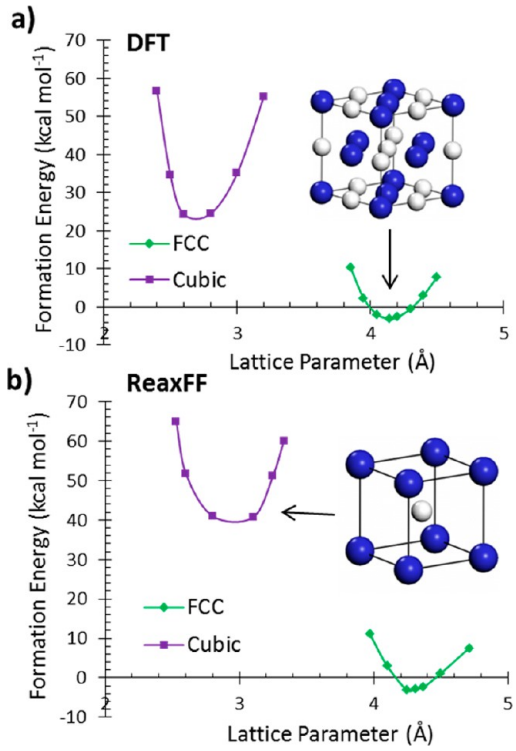


**Figure 1.** Bulk lattice expansion−compression curves for fcc and cubic PdH phases calculated with (a) DFT and (b) ReaxFF. (Insets) The structures of the (a) NaCl-type PdH phase and the (b) cubic PdH phase.

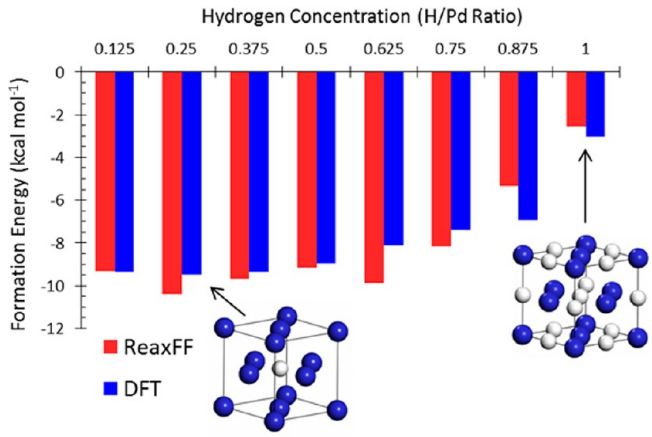


**Figure 2.** DFT and ReaxFF $PdH_x$ formation energies for hydrogen concentrations varying from $x = 0.125$ to $x = 1$. Energies are calculated relative to the $PdH_x$ ($x = 0$) structure (i.e., an expanded Pd-fcc structure) and gas phase hydrogen: $E_{form} = [E(PdH_x) - E(PdH_0)]/N_H - 1/2E(H_2)$. The insets depict orthogonal unit cells that are chemically equivalent to the triclinic unit cells employed for calculations on the $PdH_{0.25}$ and $PdH_1$ systems.

ReaxFF and DFT predict that the formation energy remains near −9 kcal $mol^{-1}$ for concentrations less than $x = 0.5$, and that the formation energy becomes significantly less favorable as additional hydrogen is added to the Pd lattice.

*Surface Adsorption Energies.* The Pd/H interaction parameters were optimized for hydrogen adsorption on Pd(111), Pd(110), and Pd(100) surface and subsurface sites. Adsorption energies were calculated relative to the clean surface and a gas phase $H_2$ molecule:


dx.doi.org/10.1021/jp411015a | J. Phys. Chem. C 2014, 118, 4967−4981

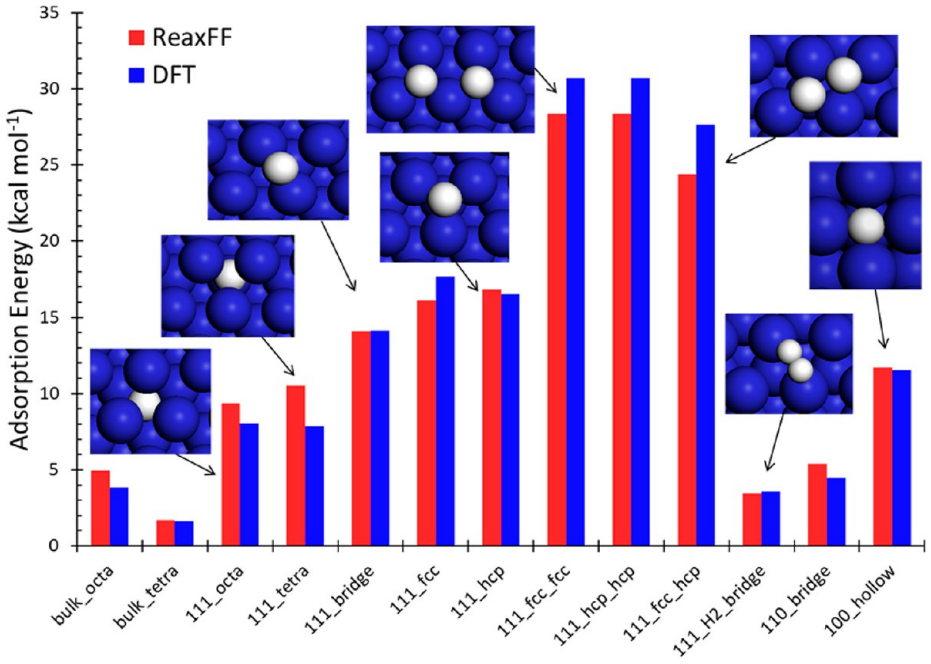


**Figure 3.** Hydrogen adsorption energies in Pd bulk and on Pd(111), Pd(110), and Pd(100) surfaces. Calculated relative to gas phase hydrogen: $E_{ads} = E_{clean} + N_H(1/2E_{H2}) - E_{H\text{-}ads/Pd}$ . (Insets) Optimized structures for H adsorption at the indicated surface sites.

$$E_{ads} = E_{clean} + N_H(1/2E_{H2}) - E_{H-ads/Pd} \quad (7)$$

where $E_{clean}$ is the energy of the clean Pd surface, $N_H$ is the number of H atoms in the cell, $E_{H2}$ is the energy of a gas phase $H_2$ molecule, and $E_{H/Pd\text{-}surf}$ is the energy of the H-adsorbed surface. Adsorption models including one adsorbed H atom resulted in a 0.11 monolayer (ML) coverage in the 3 × 3 periodic cell. We also included surface models with two H atoms adsorbed in adjacent hollow sites, resulting in a 0.22 ML coverage. This ensures that the potential can properly describe interactions between adsorbed hydrogen atoms on the Pd surface, allowing the potential to properly describe variable hydrogen coverages.

The resulting adsorption data, summarized in Figure 3, demonstrate the feasibility of the ReaxFF potential for describing hydrogen adsorption on Pd surface, subsurface, and bulk sites. At 0.11 ML, the potential yields binding energies of 16.15 kcal $mol^{-1}$ and 16.82 kcal $mol^{-1}$ for adsorption in fcc and hcp hollow sites, respectively, compared to the DFT values of 17.67 kcal $mol^{-1}$ and 16.54 kcal $mol^{-1}$. There is a repulsive interaction between H atoms adsorbed in adjacent fcc−fcc or hcp−hcp sites, reflected by lower binding energies per H atom; the respective ReaxFF adsorption energies are 28.36 kcal $mol^{-1}$ (14.18 kcal $mol^{-1}$ per H atom) and 28.35 kcal $mol^{-1}$ (14.17 kcal $mol^{-1}$ per H atom). These energies are in agreement with our respective DFT values of 30.72 kcal $mol^{-1}$ and 30.71 kcal $mol^{-1}$, and with those reported by Lopez et al.,[32] who calculated DFT-PW91 adsorption energies for fcc hollow sites of 15.45 kcal $mol^{-1}$ and 28.59 kcal $mol^{-1}$ (14.29 kcal $mol^{-1}$ per H atom) at 0.22 and 0.66 ML coverage, respectively. As stated in Section 2.2, the PW91 functional generally overbinds hydrogen on the Pd surface compared to experimental data, which is evident in the experimental fcc hollow site binding energies of 10.75 kcal $mol^{-1}$ per H atom at low coverage and 9.23 kcal $mol^{-1}$ per H atom at high coverage.[20,21] This systematic error is on the order of ∼5 kcal $mol^{-1}$, and can be empirically corrected by adjusting the ground state energy of $H_2$ to fit experimental data. We did not apply this correction, since a change in the gas phase $H_2$ energy reference will not affect qualitative adsorption trends.

*Dissociation and Migration Barriers.* In order to model the kinetic properties of hydride formation, the ReaxFF potential was trained to reproduce DFT-NEB barriers for hydrogen dissociation, surface to subsurface migration, and bulk diffusion. The ReaxFF potential energy surfaces for these processes are shown in Figure 4. As seen in Figure 4a, ReaxFF predicts that $H_2$ dissociation on the Pd(111) surface proceeds through a physisorbed $H_2$ precursor state that has an adsorption energy of 7.81 kcal $mol^{-1}$ relative to the gas phase, which precedes a dissociation barrier of 4.93 kcal $mol^{-1}$. The stability of the $H_2$ physisorbed state is reflected in the DFT data shown in Figure 3, in which we identified a local energy minimum for $H_2$ adsorption on a bridge site. This dissociation path is in qualitative agreement with the DFT-PW91 dissociation path reported by Lopez et al.[32] and reproduced in Figure 4a, which shows a precursor state with an adsorption energy of 7.1 kcal $mol^{-1}$ and a corresponding dissociation barrier of 2.1 kcal $mol^{-1}$. Figure 4b shows the ReaxFF barrier for H migration from a surface fcc hollow site to a subsurface octahedral site. ReaxFF predicts a subsurface diffusion barrier of 11.71 kcal $mol^{-1}$, in agreement with our DFT barrier of 10.42 kcal $mol^{-1}$. Finally, the potential was trained to reproduce the diffusion barrier for H migration in bulk Pd from an octahedral site to a tetrahedral site. The potential predicts adsorption energies of 4.95 kcal $mol^{-1}$ and 1.67 kcal $mol^{-1}$ in bulk octahedral and tetrahedral sites, respectively, in agreement with the respective DFT values of 3.86 kcal $mol^{-1}$ and 1.64 kcal $mol^{-1}$. As seen in Figure 4, the potential yields a barrier of 6.38 kcal $mol^{-1}$, in agreement with the DFT barrier of 5.12 kcal $mol^{-1}$. These data for adsorption and migration in bulk Pd are also in agreement with the DFT barrier of 5.07 kcal $mol^{-1}$ reported by Grönbeck and Zhdanov,[34] and the experimental diffusion barrier of 5.85 kcal $mol^{-1}$ reported by Hara et al.[28] Together, the agreement between ReaxFF and DFT for surface and bulk data


dx.doi.org/10.1021/jp411015a | J. Phys. Chem. C 2014, 118, 4967−4981

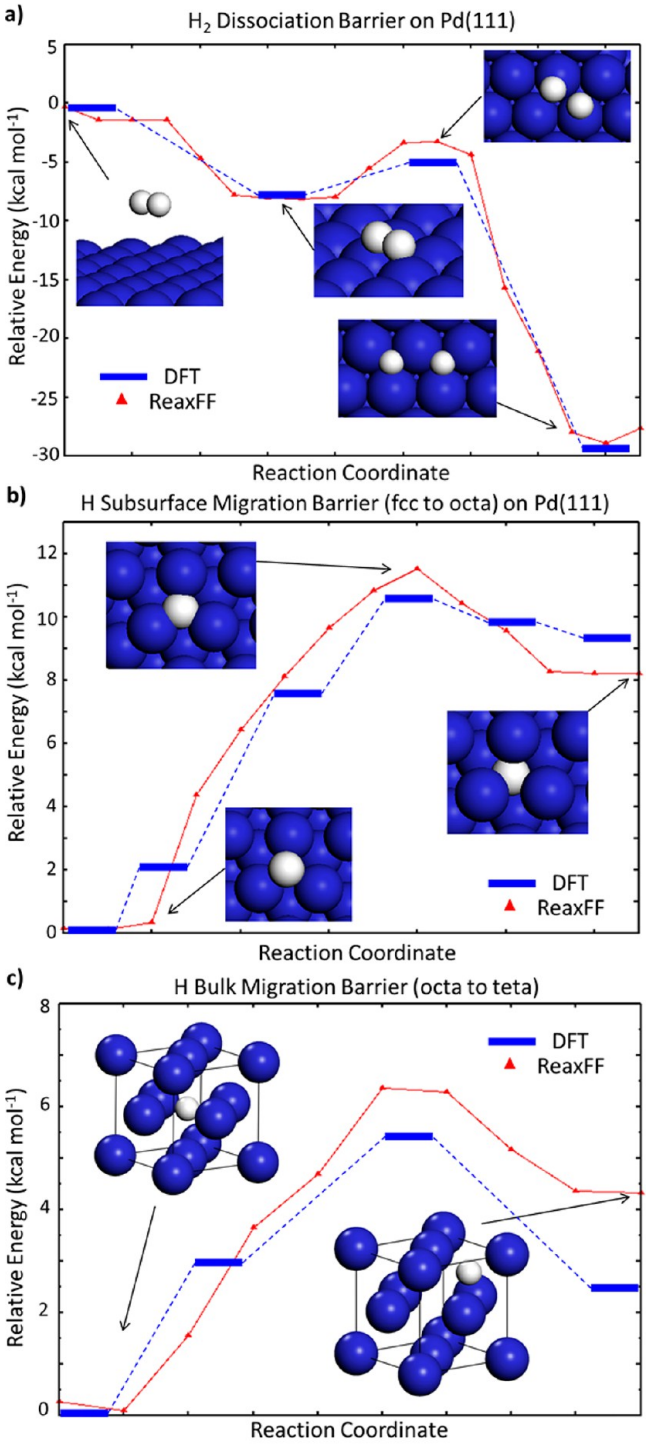


**Figure 4.** DFT (blue) and ReaxFF (red) activation barriers for (a) $H_2$ dissociation on the Pd(111) surface (DFT potential energy surface reproduced from ref 32), (b) H migration from a Pd(111) surface fcc site to a subsurface octahedral site, and (c) H migration from an octahedral site to a tetrahedral site in the bulk. (Insets) Initial structures, transition states, and final structures.

demonstrates the Pd/H potential's ability to properly model hydrogen dissociation and migration on the Pd surface, migration from Pd surface sites to subsurface sites, and diffusion in bulk Pd.

**3.2. Monte Carlo Simulations of Palladium Hydride Formation.** We applied the optimized Pd/H potential in GC-MC/MD simulations to assess the extent of hydrogen uptake in Pd bulk and clusters as a function of hydrogen pressure and temperature. Each Pd cluster simulation began with a clean Pd cluster in a 50 Å × 50 Å × 50 Å simulation box. Three spherical Pd cluster models of varying size were studied, and were constructed from the optimized fcc bulk structure. The clusters were approximately 1.0 nm, 1.5 nm, and 2.0 nm in diameter, and consisted of 43, 135, and 321 Pd atoms, respectively. A geometry optimization of the Pd clusters prior to the GC-MC/MD simulations was not necessary, as hydrogen induced restructuring of the cluster will occur during the MD relaxation steps of the simulation. Bulk simulations were initiated from an orthogonal fcc lattice consisting of 108 Pd atoms with an optimized Pd−Pd lattice spacing. The GC-MC/MD algorithm added, moved, and removed hydrogen atoms until the system reached thermodynamic equilibrium, at which point the chemical potential of hydrogen in the simulation box and the hydrogen reservoir are equal. This is demonstrated in Figure 5, which depicts the equilibration of both a cluster and a bulk MC simulation. For cluster simulations, equilibrium is reached when the system energy and the number of hydrogen atoms converges, as seen in Figure 5a. Figure 5b shows the same equilibration for bulk simulations, in which the system volume must also converge. As seen in the figure, the MC simulations typically required between 5000 and 10 000 MC iterations to converge, and were considered converged if the total energy fluctuation normalized by the number of Pd atoms in the system was less than ∼5 kcal $mol^{-1}$ over the final 1000 MC iterations. The converged system reflects the equilibrium hydrogen concentration and phase structure at the temperature and pressure specified by the chemical potential of the hydrogen reservoir.

*Surface, Subsurface, and Bulk Hydrogen Loading.* The GC-MC/MD method was used to assess the degree of hydrogen loading at surface, subsurface, and bulk-like sites in the Pd clusters. For each cluster, GC-MC/MD simulations were conducted at 300 K and at pressures ranging from $10^{-14}$ atm to $10^{-1}$ atm. We analyzed the final structure of each simulation to assess the degree of hydride formation in the surface, subsurface, and bulk-like regions of the Pd cluster as a function of hydrogen pressure. First, we calculated the radial distribution of hydrogen atoms in each cluster from the final atomic coordinates of the equilibrated system. Figure 6 shows the local density of hydrogen atoms as a function of radial distance from the center ($r$ = 0) of a 2.0 nm cluster at varying $H_2$ pressures. As expected, the H/Pd ratio progressively increases as the hydrogen pressure is increased; surface sites are first occupied at low hydrogen pressures, followed by subsurface sites, and then bulk sites. The figure shows the onset of hydrogen uptake in the bulk-like region of the cluster at $10^{-11}$ atm, and the formation of the hydride phase by $10^{-9}$ atm. This demonstrates the enhanced hydrogen binding of the Pd surface compared to the bulk, in agreement with experimental results[37,69] and with previous MC results obtained by Wolf et al.[55] and by Ruda et al.[57]

To further assess whether a phase transition occurs in the cluster, we determined the number of hydrogen atoms in the surface and bulk-like regions of the cluster by radially integrating the local hydrogen densities. This results in the data shown in Figure 7, which shows the total number of hydrogen atoms within a specified radius from the cluster center. As seen in the figure, there is a clear distinction between hydrogen loading in the bulk-like region and the surface


dx.doi.org/10.1021/jp411015a | J. Phys. Chem. C 2014, 118, 4967−4981

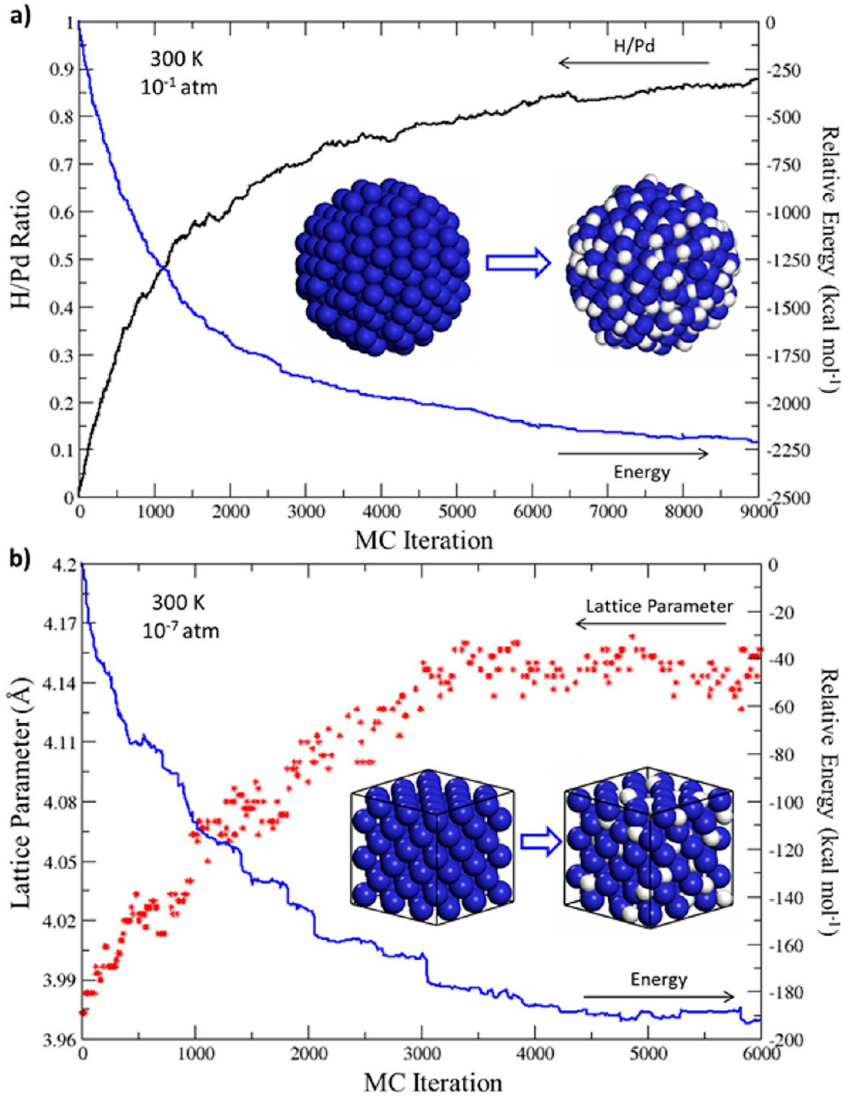


**Figure 5.** Equilibration of GC-MC/MD with (a) varying H/Pd ratio in a 2.0 nm Pd cluster at 300 K and $10^{-1}$ atm, and with (b) varying volume in Pd bulk at 300 K and $P_{H2} = 10^{-7}$ atm, where $E_{relative} = E_{system} - E_{clean} - N_H\mu_{res}$. (Insets) Initial and final system structures.

regions. The distinction between surface and subsurface regions is less clear due to the fact that the cluster models are not perfectly spherical and contain corner, edge, and facet sites that slightly vary in distance from the cluster center, which can be seen in the insets of Figure 7. This makes it difficult to distinguish between atoms adsorbed in the subsurface layer and atoms adsorbed on surface sites that are closer to the cluster center. Nevertheless, there is still a clear distinction between the bulk and surface regions, which is demonstrated by the pronounced increase in the number of hydrogen atoms near the surface of each cluster, marked by a dashed line in the figure. Using this distinction, the H/Pd ratio in the bulk-like region of each cluster can be determined as a function of pressure, thus deriving absorption isotherms that reflect hydrogen uptake in the cluster's bulk-like region. This allows for the varying phase behaviors of the bulk and surface regions to be assessed independently, as will be discussed in the following section.

*Hydrogen Absorption Isotherms.* Hydrogen absorption isotherms are shown in Figure 8a for bulk simulations at varying temperatures, and in Figure 8b,c for cluster simulations with varying cluster sizes. As seen in Figure 8a, the bulk simulations yield a clear plateau characteristic of the $\alpha$ to $\beta$ phase transition at 300 K, 400 K, and 500 K. At 300 K, the simulations yield a maximum H/Pd ratio in the $\alpha$ phase, $\alpha_{max}$, of 0.02, and a minimum H/Pd ratio in the $\beta$ phase, $\beta_{min}$, of 0.54, in agreement with the respective experimental values of $\alpha_{max} = 0.03$ and $\beta_{min} = 0.55$ reported by Yamauchi et al.[22] for hydrogen uptake in Pd-black at 303 K. At 400 and 500 K, $\alpha_{max}$ increases to 0.06 and 0.07, respectively, and $\beta_{min}$ decreases to 0.50 and 0.47, respectively. This qualitatively reproduces the experimentally observed MG narrowing with increasing temperature. We note that the isotherm-plateau predicted by ReaxFF occurs at pressures much lower than those determined experimentally,[22,26] which is caused by the overprediction of the hydrogen binding energy noted in the previous sections. At 300 K, the GC-MC/MD method predicts a plateau at $P_{H2} \sim 5.5 \times 10^{-11}$ atm, as opposed to the experimentally observed plateau near $\sim 10^{-3}$ atm. Using eq 6, these two hydrogen pressures at 300 K result in chemical potentials of $\mu_H = -63.2$ kcal mol$^{-1}$ and $\mu_H = -58.3$ kcal mol$^{-1}$, respectively. This is within the ~5 kcal mol$^{-1}$ overbinding error of the DFT-PW91 method used to train the ReaxFF potential, thus accounting for the discrepancy in plateau pressures. As stated above, the disparity between the hydrogen binding energies predicted by ReaxFF


dx.doi.org/10.1021/jp411015a | J. Phys. Chem. C 2014, 118, 4967−4981

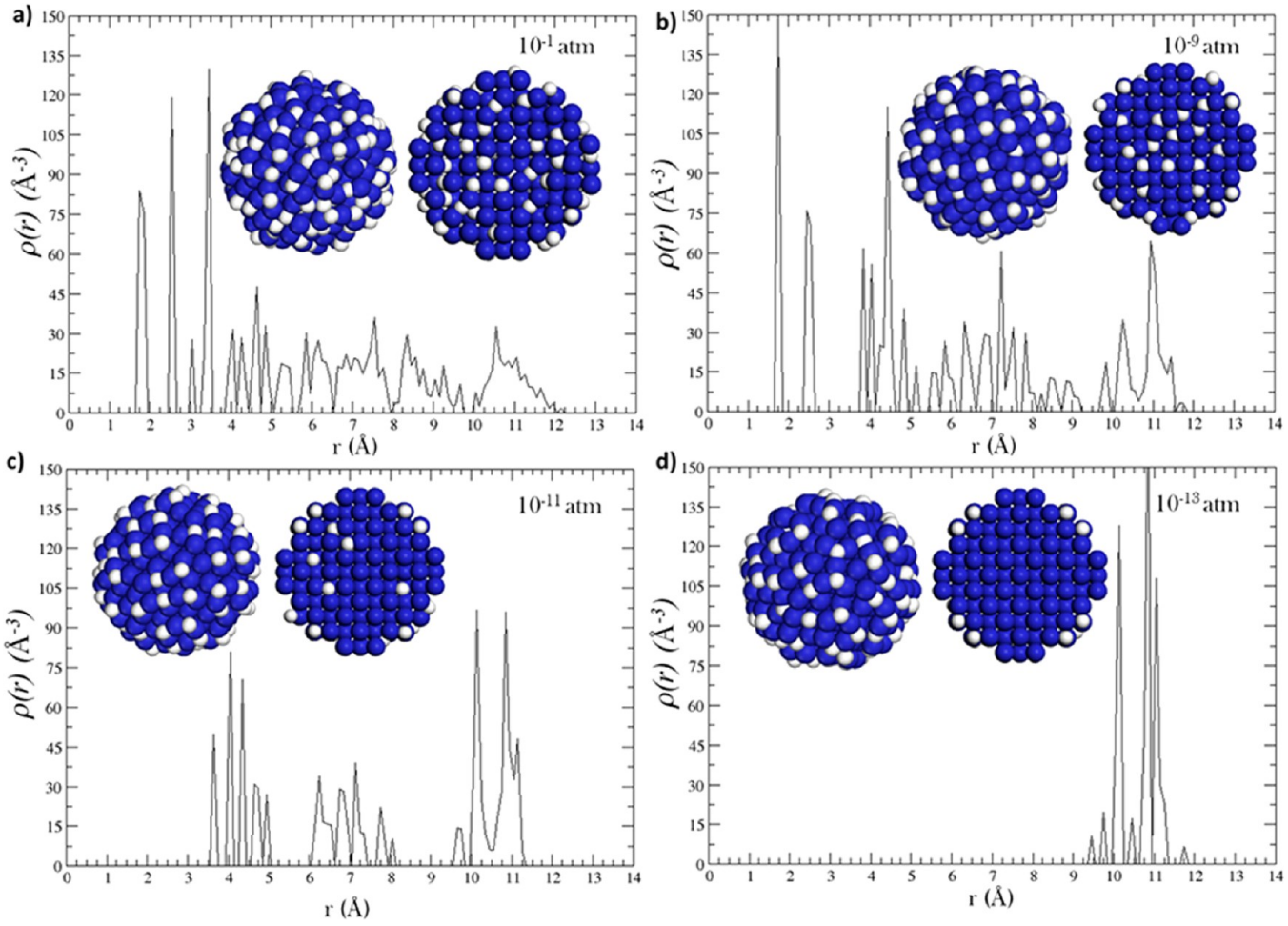


**Figure 6.** Final structure and local hydrogen densities relative to the center of the Pd cluster after GC-MC/MD simulations at $T$ = 300 K and $P$ = (a) $10^{-1}$ atm, (b) $10^{-9}$ atm, (c) $10^{-11}$ atm, and (d) $10^{-13}$ atm. (Insets) Whole structure (left) and cross section (right) of the final cluster structures after GC-MC/MD.

and experiment is the result of a systematic error in the hydrogen energy reference, and does not impact relative trends in hydrogen binding.

Absorption isotherms for 1.0 nm, 1.5 nm, and 2.0 nm Pd clusters are shown in Figure 8b,c. The H/Pd ratios shown in Figure 8b were derived using the radial distribution data shown in Figure 7, and reflect the number of hydrogen atoms in the bulk-like region of the cluster divided by the total number of Pd atoms in the cluster. The clusters display an increased hydrogen concentration in the solid solution $\alpha$ phase, and a decreased hydrogen concentration in the hydride $\beta$ phase compared to the bulk. As cluster size decreases, the $\alpha$ phase concentration increases and the $\beta$ phase concentration decreases, resulting in a narrowed MG and a sloped plateau connecting the phases, in agreement with experimental observations.[15,22,26,37] Although the cluster plateaus are sloped and narrowed compared to the bulk, each plateau retains a clear inflection point indicative of a $\alpha$ to $\beta$ phase transition. Figure 8(c) shows the total H/Pd ratios, which reflect hydrogen uptake by both the surface and bulk-like regions of each cluster. As seen in the figure, there is a high affinity for adsorption on the cluster surface, making it difficult to discern the isotherm-plateau behavior observed in the bulk-like region. This suggests that the cluster surface becomes saturated with adsorbed hydrogen at low hydrogen pressures, and the surface remains covered despite any phase transition in the bulk-like region below. Figure 8b correspondingly shows that the phase transition occurs in the bulk-like region of the clusters, indicating that the narrowing MG with decreasing cluster size is not simply the result of an increased ratio of surface to bulk sites, in agreement with the experimental observations of Eastman et al.[31] and of Wilde et al.[40]

*Lattice Expansion.* In addition to an increased H/Pd ratio, the $\alpha$ to $\beta$ transition is principally marked by an increased Pd−Pd lattice spacing. To investigate this behavior, we determined the average Pd−Pd lattice spacing for each cluster as a function of hydrogen pressure, as shown in Figure 9. This was accomplished by calculating the Pd−Pd radial pair distribution function, $g(r)$, from the final atomic coordinates of the equilibrated GC-MC/MD cluster simulations. As seen in the figure, the peaks in the pair distribution function retain the characteristic fcc lattice spacing of the clean cluster, and broaden at higher hydrogen pressures. As such, the equilibrium fcc lattice spacing was approximated by taking the weighted average over the first $g(r)$ peak. The resulting lattice spacings, shown in Figure 9, demonstrate a discernible increase in the fcc lattice constant as $H_2$ pressure increases, indicating that the phase transition occurs in all three clusters. The maximum lattice spacing of the $\alpha$ phase increases and the minimum lattice spacing of the $\beta$ phase decreases with decreasing cluster size.


dx.doi.org/10.1021/jp411015a | J. Phys. Chem. C 2014, 118, 4967−4981

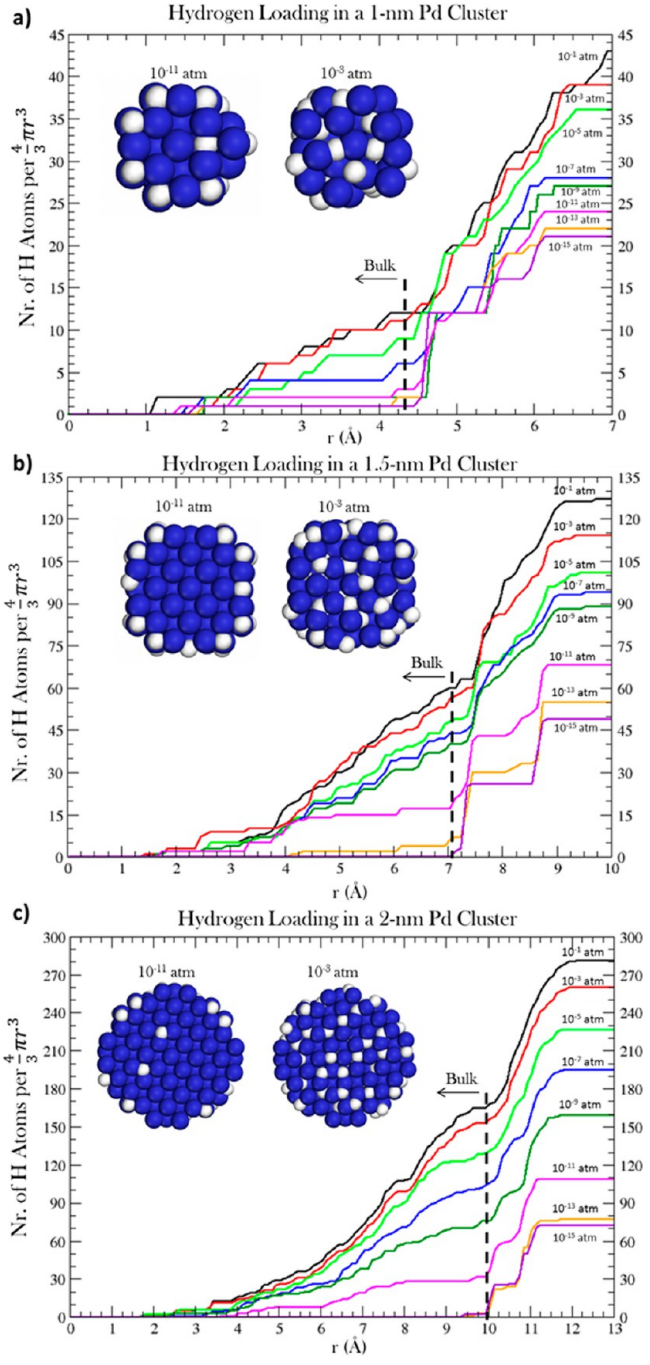


**Figure 7.** Radial distribution of hydrogen atoms in (a) a 1.0 nm Pd cluster, (b) a 1.5 nm Pd cluster, and (c) a 2.0 nm Pd cluster after GC-MC/MD simulations at 300 K and at $P = 10^{-15}$ atm (purple), $P = 10^{-13}$ atm (orange), $P = 10^{-11}$ atm (magenta), $P = 10^{-9}$ atm (dark green), $P = 10^{-7}$ atm (blue), $P = 10^{-5}$ atm (light green), $P = 10^{-3}$ atm (red), $P = 10^{-1}$ atm (black). (Insets) Cross section of the center of the cluster exposing a (100) facet after GC-MC/MD at $10^{-11}$ atm and $10^{-3}$ atm.

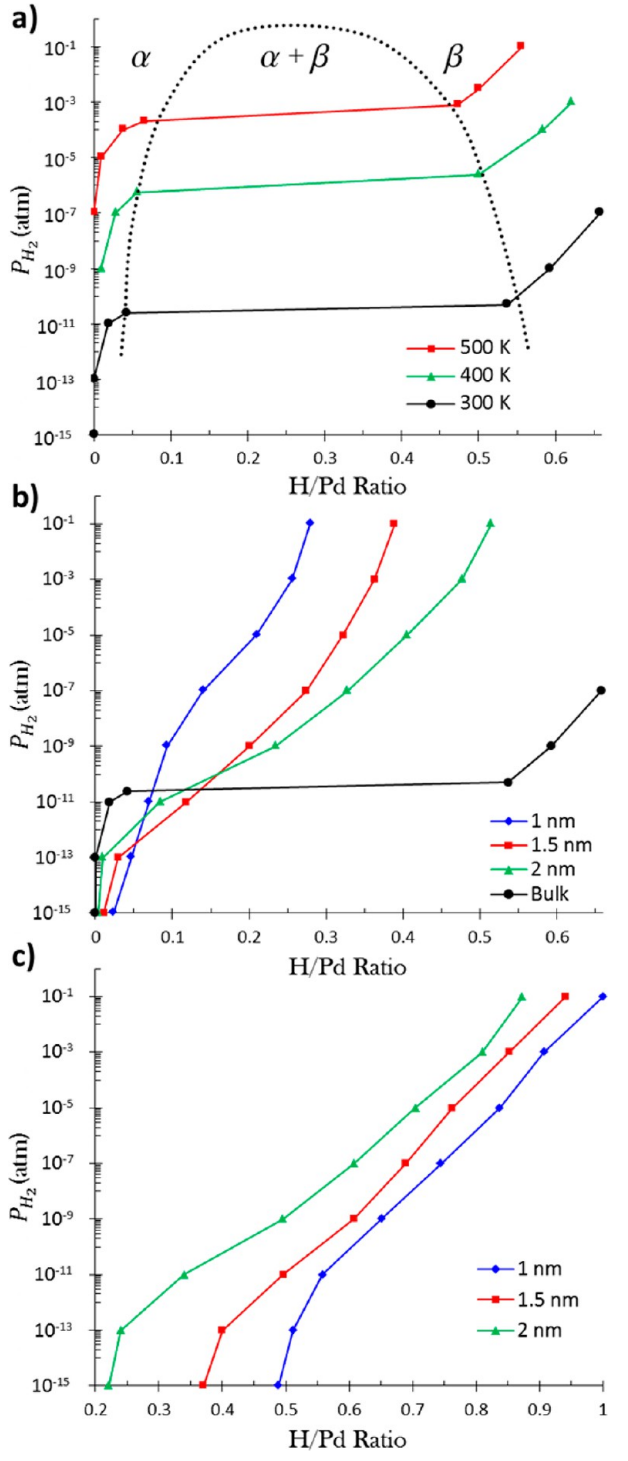


**Figure 8.** Hydrogen absorption isotherms for (a) Pd bulk, (b) the bulk-like region of Pd clusters at 300 K, and (c) the entire Pd cluster (including hydrogen in both bulk and surface regions) at 300 K. The dashed line in (a) is an estimated delineation of the $\alpha/\beta$ phase boundary.

This is in agreement with the experimental XRD trend in lattice expansion reported by Ingham et al.,[17] who likewise found that the phase transition occurs in naked clusters that are as small as ~1.7 nm in diameter. The lattice parameters for bulk simulations are also summarized in Table 2, which contains the minimum and maximum lattice parameters obtained for the $\alpha$ and $\beta$ phases at 300 K, 400 K, and 500 K. The minimum bulk lattice parameter of the $\beta$ phase decreases with increasing temperature, indicating the closure of the MG as the system approaches the critical temperature. As expected, the maximum and minimum lattice parameters in the clusters approach the values obtained for the bulk as cluster size increases.

*Discussion.* These results help clarify the role of surface and bulk-like regions during hydride formation in Pd clusters. We observe that the phase transition occurs in the bulk-like region


dx.doi.org/10.1021/jp411015a | J. Phys. Chem. C 2014, 118, 4967−4981

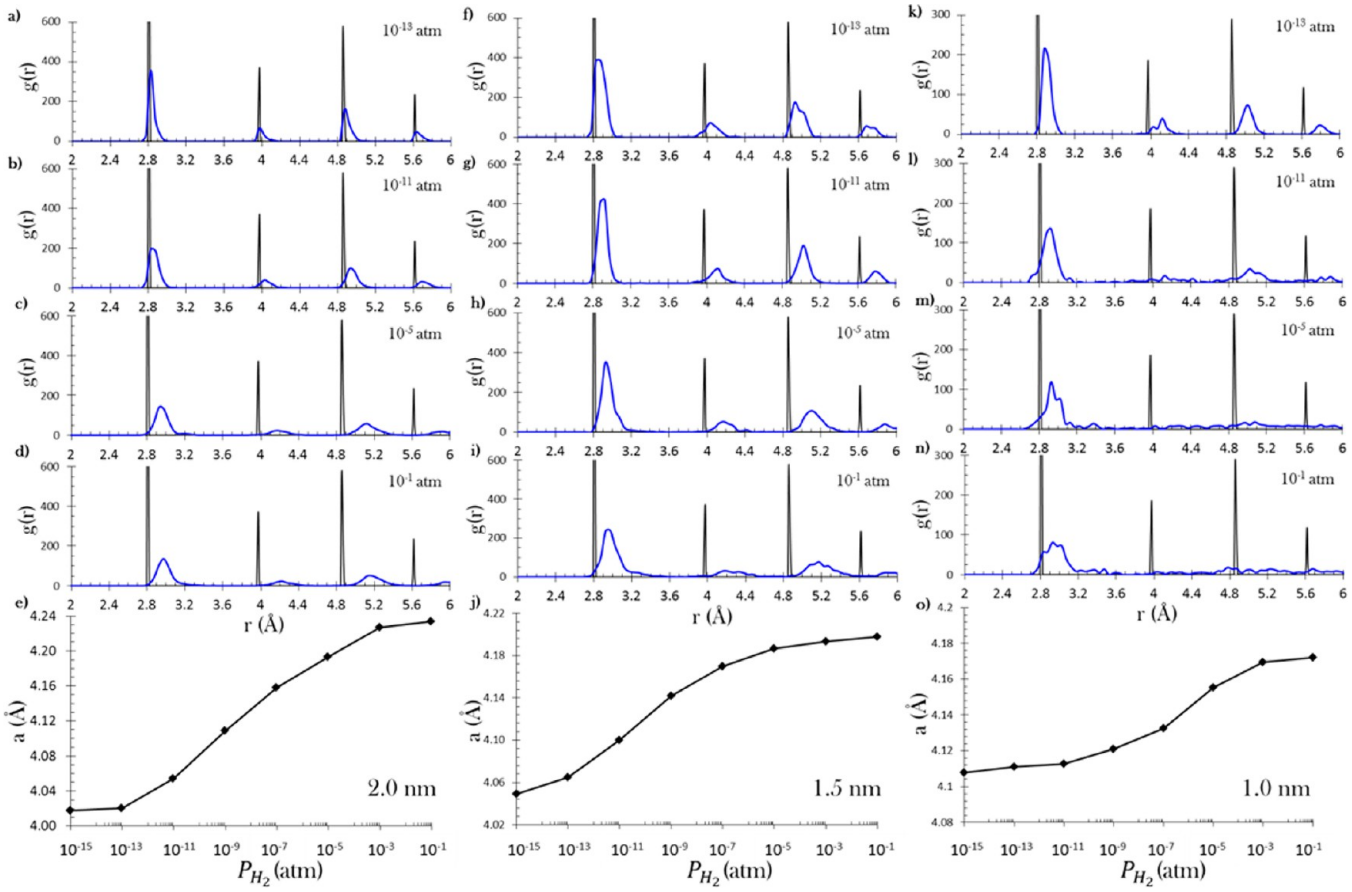


**Figure 9.** Pd−Pd pair distribution functions, $g(r)$, after GC-MC/MD equilibration in (a−d) a 2.0 nm cluster, (h−i) a 1.5 nm cluster, and (m−n) a 1.0 nm cluster. The $g(r)$ represented by a black line corresponds to the Pd−Pd pair distribution of the clean cluster prior to GC-MC/MD. (e,j,o) Average fcc lattice constants derived from pair distribution functions for (e) the 2.0 nm cluster, (j) the 1.5 nm cluster, and (o) the 1.0 nm cluster.

**Table 2. Maximum and Minimum Recorded H/Pd Ratios and Lattice Parameters in Bulk Simulations at 300 K, 400 K, and 500 K**

| 300 K | $P_{H2}$ (atm) | H/Pd ratio | lattice parameter (Å) |
|---|---|---|---|
| $\alpha$ | $1 \times 10^{-13}$ | 0.0 | 3.97 |
| $\alpha_{max}$ | $2.4 \times 10^{-11}$ | 0.02 | 3.99 |
| $\beta_{min}$ | $5 \times 10^{-11}$ | 0.54 | 4.15 |
| $\beta$ | $1 \times 10^{-1}$ | 0.88 | 4.24 |
| 400 K | $P_{H2}$ (atm) | H/Pd ratio | lattice parameter (Å) |
| $\alpha$ | $1 \times 10^{-9}$ | 0.0 | 3.97 |
| $\alpha_{max}$ | $5.5 \times 10^{-7}$ | 0.06 | 3.99 |
| $\beta_{min}$ | $2.5 \times 10^{-6}$ | 0.51 | 4.13 |
| $\beta$ | $1 \times 10^{-1}$ | 0.66 | 4.18 |
| 500 K | $P_{H2}$ (atm) | H/Pd ratio | lattice parameter (Å) |
| $\alpha$ | $1 \times 10^{-7}$ | 0.0 | 3.97 |
| $\alpha_{max}$ | $2 \times 10^{-4}$ | 0.07 | 3.99 |
| $\beta_{min}$ | $8 \times 10^{-4}$ | 0.47 | 4.12 |
| $\beta$ | $1 \times 10^{-1}$ | 0.56 | 4.16 |

of Pd clusters, and that the MG remains open for naked clusters as small as 1.0 nm in diameter. This supports the conclusion of both Wilde et al.,[40] who found that the enhanced hydrogen uptake in the solid solution phase occurs in the bulk-like region (as opposed to at surface sites), and with Eastman et al.,[31] who found that the narrowing MG in clusters cannot be attributed to a varying phase behavior in the surface/subsurface region. It also supports the conclusions of Ingham et al.,[17] who argue that the closing of the MG in small clusters reported in the literature[15,16] is the result of surface strain affecting absorption in the bulk-like region of the clusters. Our results show that the surface of the Pd cluster becomes saturated with hydrogen even at low pressures, and that the experimental trends related to cluster size are retained when these sites are excluded from the absorption isotherms, indicating that the size-dependent absorption behavior is associated with the bulk-like region of the cluster, in agreement with Wilde et al.[40] Although increased uptake occurs in the cluster bulk, it can be attributed to the effects of adsorbate bonding at the cluster surface. Ingham et al.[17] posit that Pd−Pd bonds between the surface and bulk-like region are weakened by Pd-adsorbate bonds on the surface. As surface Pd atoms form bonds to adsorbates, fewer electrons are available to fill Pd−Pd bonding orbitals between surface and subsurface Pd atoms. Such weakening of subsurface Pd−Pd bonds allows the bulk region to more easily expand to accommodate hydrogen absorption, thus making hydrogen absorption in the bulk more favorable. Since smaller clusters have a larger surface to volume ratio, this effect becomes increasingly more important as cluster size decreases, leading to a narrowed MG for smaller clusters. This effect will be magnified by strongly interacting cluster-stabilizers,[18] such as polymer matrices, surfactants, and oxide supports, thus leading to the complete closure of the MG in small clusters. The agreement between the literature and the results of the MC simulations demonstrates the applicability of the Pd/H potential, as well as the feasibility of the GC-MC/MD method


dx.doi.org/10.1021/jp411015a | J. Phys. Chem. C 2014, 118, 4967−4981

for investigating the thermodynamic stability of hydride phases in Pd bulk and clusters.

**3.3. Molecular Dynamics Simulations of Hydrogen Dissociation and Diffusion.** In addition to thermodynamic properties, the kinetics of hydrogen uptake and diffusion have been extensively investigated,[3,5,28,29,70−73] as a detailed understanding of hydrogen transport properties in Pd is essential to designing Pd-based devices with optimal absorption−desorption kinetics. The Pd/H potential developed here utilizes hydrogen parameters that are invariant between hydrogen in the gas phase, adsorbed on the surface, or dissolved in the bulk. This allows the potential to model dissociative hydrogen adsorption and diffusion into the bulk, which can help assess the kinetic properties of hydrogen transport at an atomistic level. To demonstrate this, we applied the Pd/H potential in molecular dynamics simulations to investigate the kinetics of hydrogen uptake by clusters of varying size, as well as to derive diffusion coefficients for hydrogen diffusion in the bulk at varying concentrations and temperatures. These results are compared to experimental studies, demonstrating the capabilities and limitations of the Pd/H potential for describing kinetics. MD simulations in this study were conducted in the NVT ensemble using the velocity Verlet method[74] with a time step of 0.25 fs. A Berendsen thermostat[75] with a damping constant of 100 fs maintained temperature control throughout the simulation.

*$H_2$ Dissociation and Absorption in Pd Clusters.* To model the kinetics of hydrogen dissociation and absorption in clusters, we conducted MD simulations for a duration of 250 ps, in which each simulation began with a $H_2$ gas phase surrounding a single Pd cluster. This was conducted for three spherical cluster sizes: a 1.0 nm cluster consisting of 43 Pd atoms, a 1.5 nm cluster consisting of 135 Pd atoms, and a 2.0 nm cluster consisting of 321 Pd atoms. The ratio of Pd to H atoms in the simulation cell affects the overall amount of hydrogen that can be absorbed by the clusters. Correspondingly, we populated each simulation cell with a stoichiometric 1:1 Pd/H ratio to ensure that the cluster can become saturated with H atoms. Also, the pressure of hydrogen in the gas phase affects the kinetics of hydrogen absorption. Therefore, the dimensions of the simulation cells were chosen such that each Pd cluster was exposed to an equivalent initial hydrogen pressure. The initial simulation pressure was estimated from the number of hydrogen molecules in the gas phase using the ideal gas law, yielding a pressure of ∼5.4 MPa in cubic simulation cells with side-lengths of 38 Å, 56 Å, and 75 Å for the 1.0 nm, 1.5 nm, and 2.0 nm clusters, respectively. A temperature of 1250 K was employed for all simulations, which was selected because it is high enough to allow rapid dissociation and diffusion in the time frame of the simulation, yet is still below the melting point of Pd metal. The populations of $H_2$ molecules and H atoms either present in the gas phase or adsorbed on the Pd cluster were recorded at 25 fs intervals, allowing the hydride formation process to be tracked as a function of simulation time.

Hydride formation in Pd clusters proceeds through a core−shell mechanism, in which a hydride shell forms at the surface and progresses toward the center of the cluster.[29] Hydride formation is limited by hydrogen diffusion through the hydride shell to the metallic core, and the size-dependent kinetics described by this model have been investigated theoretically by Zhdanov et al.[70] and experimentally by Langhammer et al.[29] Zhdanov et al. used Monte Carlo simulations to demonstrate a power-law relationship relating the time required to reach hydrogen saturation when forming a hydride phase to cluster size: $t_{1/2} \sim d^Z$, where $t_{1/2}$ is half the time required to reach saturation in the cluster, $d$ is the cluster diameter, and $Z$ is a proportionality constant. They predict that $Z = 2.0$ in the ideal case of diffusion limited hydride formation, and that $Z$ increases to as much as 3.0 depending on diffusion dynamics and cluster geometry. This is corroborated by the experimental results of Langhammer et al., who compared hydride formation rates in samples containing clusters with average diameters of 1.81 nm, 2.47 nm, and 5.35 nm, finding that $Z = 2.9$ at 303 K.

We conducted MD simulations, summarized in Figure 10, to determine whether the power law relation for the size-dependent kinetics of hydrogen absorption is retained by the Pd/H potential. Since these simulations were conducted at high temperatures, we expect that the small dissociation barrier (∼2 kcal mol$^{-1}$) will be readily overcome, and that the higher subsurface diffusion barrier (∼10 kcal mol$^{-1}$) will be rate limiting. As seen in the figure, the Pd/H potential yields a value of $Z = 1.92$, in agreement with the power-law scaling predicted by Zhdanov et al. for diffusion limited hydrogen uptake in Pd clusters. This, in conjunction with the experimental result of Langhammer et al., supports the core−shell model for hydride formation in clusters, in which the rate-limiting step is hydrogen diffusion to the metallic core through a growing hydride surface shell.

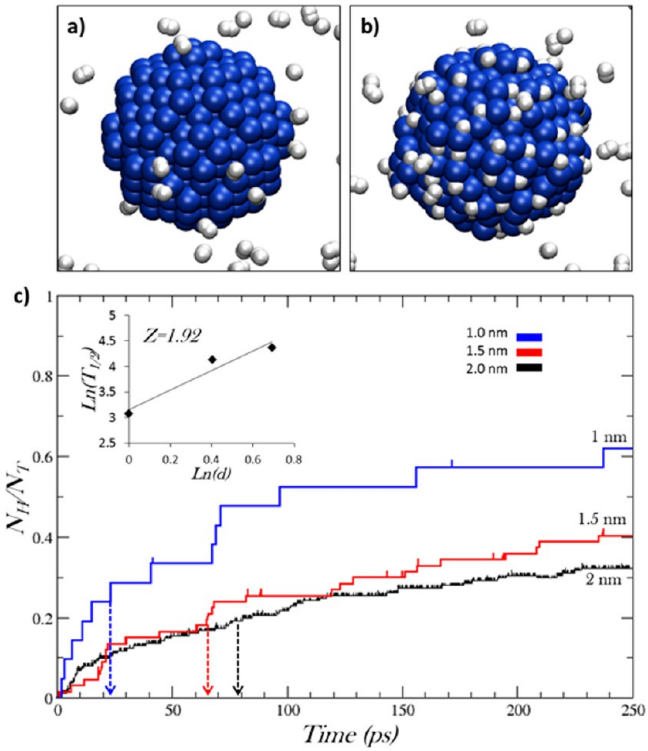


**Figure 10.** (a) Initial and (b) final structure of a 250 ps NVT-MD simulation of hydrogen adsorption at 1250 K in a 2.0 nm cluster. (c) Number of hydrogen atoms adsorbed from the gas phase normalized by the total number of hydrogen atoms. Arrows mark the time required to reach half of the final hydrogen saturation point, $t_{1/2}$ . (Inset) $t_{1/2}$ plotted against cluster diameter.

*Hydrogen Diffusion in Bulk Pd.* To derive diffusion coefficients for hydrogen diffusion in bulk Pd, we conducted NVT-MD simulations in which hydrogen was initially loaded in a fcc lattice at varying concentrations. The simulation box


dx.doi.org/10.1021/jp411015a | J. Phys. Chem. C 2014, 118, 4967−4981

consisted of 256 Pd atoms in a cubic cell with periodic boundary conditions in all three directions. Octahedral sites were randomly populated with 8, 64, or 128 H atoms, yielding H/Pd ratios of 0.03, 0.25, and 0.5, respectively. A conjugate gradient energy minimization was performed prior to each simulation to allow the simulation cell size and hydrogen coordinates to relax, thus mitigating simulation artifacts caused by high energy contacts in the initial geometry.

Diffusion coefficients were calculated from the average mean-square displacement (MSD) of hydrogen atoms, which was determined from the atomic coordinates of the system that were archived after every 0.025 ps. Diffusion coefficients were calculated from the slope of the MSD curve using the well-known relation: MSD = $6Dt$, where $D$ is the diffusion coefficient and $t$ is time. This is summarized in Figure 11 for all three hydrogen concentrations at 500 K, 550 K, 650 K, and 750 K. The apparent diffusion barrier can be determined using an Arrhenius relationship: $D = D_o \exp[-E_d/(RT)]$, where $D$ is the diffusion coefficient determined from the MSD data, $D_o$ is the Arrhenius pre-exponential factor, $E_d$ is the apparent diffusion barrier, $R$ is the gas constant, and $T$ is temperature. This is demonstrated in Figure 12, where a linear regression was employed to determine the pre-exponential factor and hydrogen diffusion barrier at each concentration. The results, tabulated in Table 3 along with experimental comparisons, show that the diffusion barrier increases from 6.87 kcal mol$^{-1}$ at H/Pd = 0.03, to 7.55 kcal mol$^{-1}$ and 8.32 kcal mol$^{-1}$ at H/Pd = 0.25 and 0.5, respectively. As shown in Figure 12, the diffusion coefficients increase with decreasing hydrogen concentration, moving toward the experimentally determined[28] dilute limit shown in the figure. Despite approaching the experimentally determined dilute limit, the Pd/H potential still systemically under-predicts hydrogen diffusion coefficients compared to the experimental barriers reported Hara et al.[28] However, the magnitude of this deviation can be attributed to the fact that ReaxFF overpredicts the hydrogen diffusion barrier, shown in Figure 4, by ~2 kcal mol$^{-1}$, which is within the expected accuracy of the ReaxFF method. The agreement between ReaxFF and experiment demonstrates that the Pd/H potential can be used to derive hydrogen diffusion properties in bulk Pd over a variety of temperatures and concentrations.

Together, the MD results presented above demonstrate that the ReaxFF potential can accurately represent the interaction between hydrogen and Pd both at the gas/surface interface and in the bulk. This demonstrates the capabilities of the potential for investigating the kinetic properties of hydrogen uptake and diffusion in both cluster and bulk systems.

## 4. CONCLUSION

Palladium can readily dissociate and absorb hydrogen from the gas phase, making it a candidate for use in hydrogen storage devices, separation membranes, and hydrogenation catalysts. Optimizing the design of these devices requires an extensive knowledge of both kinetic and thermodynamic influences affecting hydrogen transport at the atomistic scale. To aid this effort, we derived a ReaxFF interaction potential for Pd/H from an extensive set of DFT data for both bulk and surface properties. Using this potential, we conducted GC-MC/MD simulations to derive theoretical hydrogen absorption isotherms in Pd bulk and clusters, thus assessing the contributing roles of surface, subsurface, and bulk regions during the size-dependent transition between the solid solution $\alpha$ phase and the hydride $\beta$ phase. We determined that the narrowing

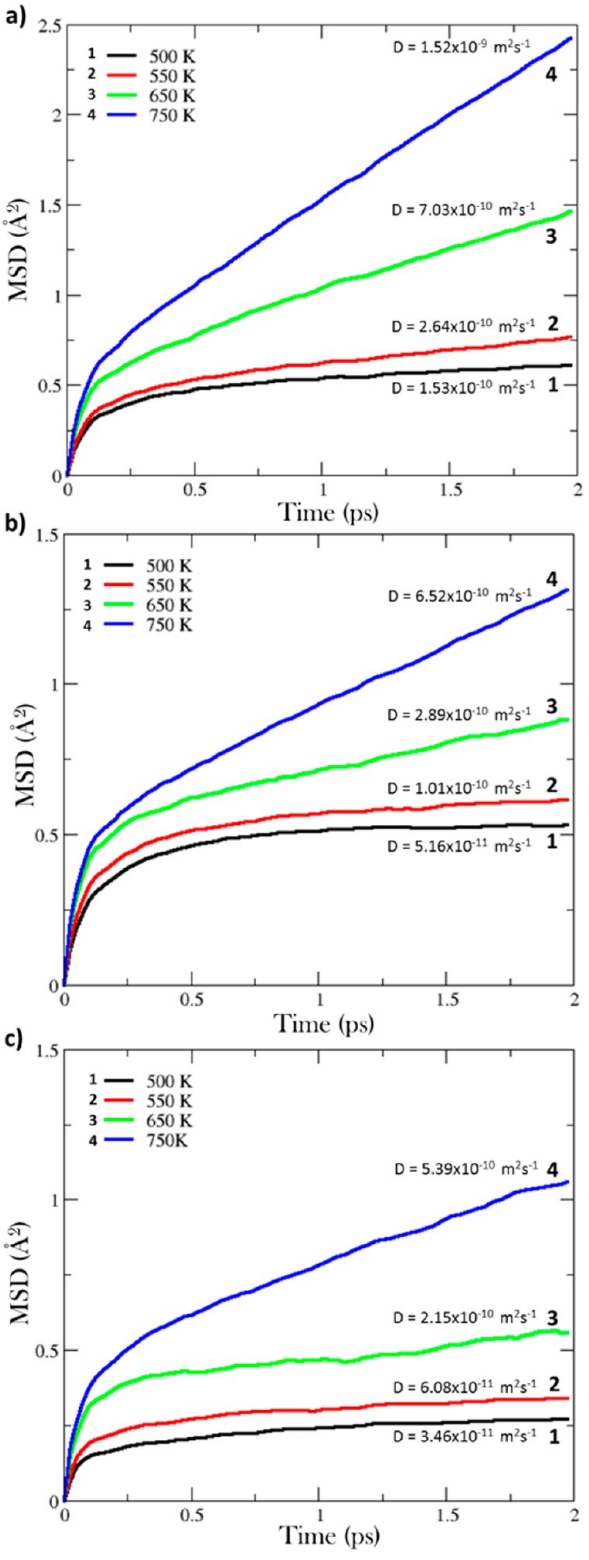


**Figure 11.** Mean-square displacements of hydrogen during MD-NVT simulations of $PdH_x$ bulk for (a) $x$ = 0.03, (b) $x$ = 0.25, and (c) $x$ = 0.5.

hydrogen miscibility gap in Pd clusters of decreasing size is related to an increased solubility in the bulk-like region of the cluster, and that the miscibility gap remains open for naked clusters at small as 1.0 nm in diameter, in agreement with previous experimental observations.[17] Additionally, we con-


dx.doi.org/10.1021/jp411015a | J. Phys. Chem. C 2014, 118, 4967−4981

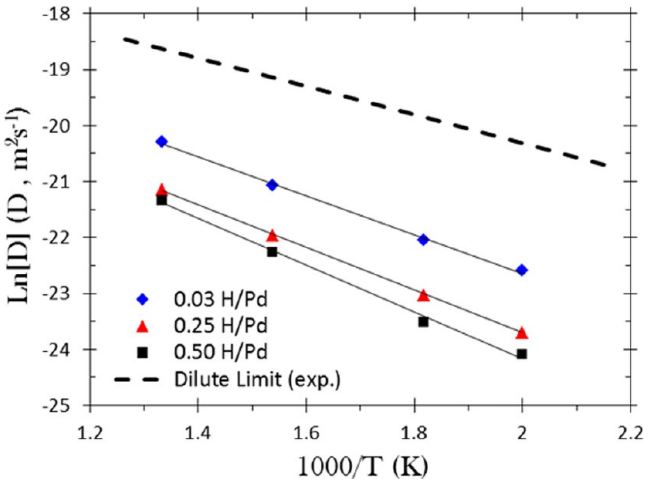


**Figure 12.** Arrhenius relationship between diffusion coefficients and temperature obtained from MD-NVT simulations at varying hydrogen concentrations. The dashed line shows the experimental dilute limit reported in ref 28.

**Table 3. Activation Barriers ($E_d$) and Pre-exponential Factors ($D_0$) for Hydrogen Diffusion in Bulk Pd**

| H/Pd | $E_d$ (kcal mol$^{-1}$) | $D_0$ ($10^{-6}$ m$^2$ s$^{-1}$) |
|---|---|---|
| 0.5 | 8.32 | 0.137 |
| 0.25 | 7.55 | 0.102 |
| 0.03 | 6.87 | 0.144 |
| *0.02−0.05 (500 kPa)*[a] | *6.26* | *0.553* |
| *0.04*[a] | *5.86* | *0.385* |
| *dilute limit*[a] | *5.04* | *0.240* |

[a]Experimental barriers and pre-exponentials from ref 28.

ducted NVT simulations of the dissociative adsorption of hydrogen from the gas phase, and of hydrogen diffusion in the bulk. The size-dependent kinetics of hydrogen absorption from the gas phase, as well as bulk diffusion coefficients, determined from these simulations are in agreement with experimental results,[28,29] demonstrating the capability of the ReaxFF potential for modeling hydrogen transport between gas and solid phases. The corroboration between experiment and ReaxFF both validates the Pd/H interaction potential for treating the complex phase behavior of PdH, as well as demonstrates the ability of ReaxFF to assess thermodynamic and kinetic influences on phase behavior at the atomic scale through GC-MC and MD methods.

## ■ ASSOCIATED CONTENT

### Supporting Information

A full Pd/H force-field parameter set in ReaxFF input format is provided. This material is available free of charge via the Internet at http://pubs.acs.org.

## ■ AUTHOR INFORMATION

### Corresponding Authors

*E-mail: mjanik@psu.edu; Phone: (814) 863-9366 (M.J.J).
*E-mail: acv13@psu.edu; Phone: (814) 863-6277 (A.C.T.v.D.).

### Notes

The authors declare no competing financial interest.

## ■ ACKNOWLEDGMENTS

This research was supported by funding from the National Science Foundation Grant CBET-1032979.

## ■ REFERENCES

(1) Yamauchi, M.; Kitagawa, H. Hydrogen Absorption of the Polymer-Coated Pd Nanoparticle. *Synth. Met.* **2005**, *153*, 353−356.
(2) Yamauchi, M.; Kobayashi, H.; Kitagawa, H. Hydrogen Storage Mediated by Pd and Pt Nanoparticles. *Chem. Phys. Chem.* **2009**, *10*, 2566−2576.
(3) Lebouin, C.; Soldo, Y.; Grigoriev, S. A.; Guymont, M.; Millet, P. Kinetics of Hydrogen Sorption by Palladium Nanoparticles. *Int. J. Hydrogen Energy* **2013**, *38*, 966−972.
(4) Cheon, Y. E.; Suh, M. P. Enhanced Hydrogen Storage by Palladium Nanoparticles Fabricated in a Redox-Active Metal−Organic Framework. *Angew. Chem., Int. Ed.* **2009**, *48*, 2899−2903.
(5) Michalak, W. D.; Miller, J. B.; Alfonso, D. R.; Gellman, A. J. Uptake, Transport, and Release of Hydrogen from Pd(100). *Surf. Sci.* **2012**, *606*, 146−155.
(6) Kamakoti, P.; Morreale, B. D.; Ciocco, M. V.; Howard, B. H.; Killmeyer, R. P.; Cugini, A. V.; Sholl, D. S. Prediction of Hydrogen Flux through Sulfur-Tolerant Binary Alloy Membranes. *Science* **2005**, *307*, 569−573.
(7) Hatlevik, Ø.; Gade, S. K.; Keeling, M. K.; Thoen, P. M.; Davidson, A. P.; Way, J. D. Palladium and Palladium Alloy Membranes for Hydrogen Separation and Production: History, Fabrication Strategies, and Current Performance. *Sep. Purif. Technol.* **2010**, *73*, 59−64.
(8) Borodziński, A.; Bond, G. C. Selective Hydrogenation of Ethyne in Ethene-Rich Streams on Palladium Catalysts. Part 1. Effect of Changes to the Catalyst During Reaction. *Catal. Rev.* **2006**, *48*, 91−144.
(9) Borodziński, A.; Bond, G. C. Selective Hydrogenation of Ethyne in Ethene-Rich Streams on Palladium Catalysts, Part 2: Steady-State Kinetics and Effects of Palladium Particle Size, Carbon Monoxide, and Promoters. *Catal. Rev.* **2008**, *50*, 379−469.
(10) Chizallet, C.; Bonnard, G..; Krebs, E.; Bisson, L.; Thomazeau, C..; Raybaud, P. Thermodynamic Stability of Buta-1,3-diene and But-1-ene on Pd(111) and (100) Surfaces under $H_2$ Pressure: A DFT Study. *J. Phys. Chem. C* **2011**, *115*, 12135−12149.
(11) Teschner, D.; Borsodi, J.; Wootsch, A.; Révay, Z.; Hävecker, M.; Knop-Gericke, A.; Jackson, S. D.; Schlögl, R. The Roles of Subsurface Carbon and Hydrogen in Palladium-Catalyzed Alkyne Hydrogenation. *Science* **2008**, *320*, 86−89.
(12) Teschner, D.; Borsodi, J.; Kis, Z.; SzentmiklÓsi, L.; Révay, Z.; Knop-Gericke, A.; SchlÖgl, R.; Torres, D.; Sautet, P. Role of Hydrogen Species in Palladium-Catalyzed Alkyne Hydrogenation. *J. Phys. Chem. C* **2010**, *114*, 2293−2299.
(13) Ludwig, W.; Savara, A.; Madix, R. J.; Schauermann, S.; Freund, H. Subsurface Hydrogen Diffusion into Pd Nanoparticles: Role of Low-Coordinated Surface Sites and Facilitation by Carbon. *J. Phys. Chem. C* **2012**, *116*, 3539−3544.
(14) Jewell, L. L.; Davis, B. H. Review of Absorption and Adsorption in the Hydrogen−Palladium System. *Appl. Catal. A: Gen.* **2006**, *310*, 1−15.
(15) Suleiman, M.; Jisrawi, N. M.; Dankert, O.; Reetz, M. T.; Bähtz, C.; Kirchheim, R.; Pundt, A. Phase Transition and Lattice Expansion During Hydrogen Loading of Nanometer Sized Palladium Clusters. *J. Alloys Compd.* **2003**, *356−357*, 644−648.
(16) Konopsky, V. N.; Basmanov, D. V.; Alieva, E. V.; Sekatskii, S. K.; Dietler, G. Size-Dependent Hydrogen Uptake Behavior of Pd Nanoparticles Revealed by Photonic Crystal Surface Waves. *Appl. Phys. Lett.* **2012**, *100*, 083108−083104.
(17) Ingham, B.; Toney, M. F.; Hendy, S. C.; Cox, T.; Fong, D. D.; Eastman, J. A.; Fuoss, P. H.; Stevens, K. J.; Lassesson, A.; Brown, S. A.; et al. Particle Size Effect of Hydrogen-Induced Lattice Expansion of Palladium Nanoclusters. *Phys. Rev. B* **2008**, *78*, 245408−245413.

(18) Suleiman, M.; Faupel, J.; Borchers, C.; Krebs, H. U.; Kirchheim, R.; Pundt, A. Hydrogen Absorption Behaviour in Nanometer Sized Palladium Samples Stabilised in Soft and Hard Matrix. *J. Alloys Compd.* **2005**, *404*−*406*, 523−528.
(19) Behm, R. J.; Christmann, K.; Ertl, G. Adsorption of Hydrogen on Pd(100). *Surf. Sci.* **1980**, *99*, 320−340.
(20) Conrad, H.; Ertl, G.; Latta, E. E. Adsorption of Hydrogen on Palladium Single Crystal Surfaces. *Surf. Sci.* **1974**, *41*, 435−446.
(21) Engel, T.; Kuipers, H. A Molecular-Beam Investigation of the Scattering, Adsorption and Absorption of $H_2$ and $D_2$ from/on/in Pd(111). *Surf. Sci.* **1979**, *90*, 162−180.
(22) Yamauchi, M.; Ikeda, R.; Kitagawa, H.; Takata, M. Nanosize Effects on Hydrogen Storage in Palladium. *J. Phys. Chem. C* **2008**, *112*, 3294−3299.
(23) Dong, W.; Hafner, J. $H_2$ Dissociative Adsorption on Pd(111). *Phys. Rev. B* **1997**, *56*, 15396−15403.
(24) Dong, W.; Ledentu, V.; Sautet, P.; Eichler, A.; Hafner, J. Hydrogen Adsorption on Palladium: A Comparative Theoretical Study of Different Surfaces. *Surf. Sci.* **1998**, *411*, 123−136.
(25) Zhao, Y.; Tian, D. Hydrogen Adsorption and Dissociation on $Pd_{19}$ Cluster Using Density Functional Calculations. *Comp. Theor. Chem.* **2012**, *991*, 40−43.
(26) Kishore, S.; Nelson, J. A.; Adair, J. H.; Eklund, P. C. Hydrogen Storage in Spherical and Platelet Palladium Nanoparticles. *J. Alloys Compd.* **2005**, *389*, 234−242.
(27) Moreno, M.; Ibañez, F. J.; Jasinski, J. B.; Zamborini, F. P. Hydrogen Reactivity of Palladium Nanoparticles Coated with Mixed Monolayers of Alkyl Thiols and Alkyl Amines for Sensing and Catalysis Applications. *J. Am. Chem. Soc.* **2011**, *133*, 4389−4397.
(28) Hara, S.; Caravella, A.; Ishitsuka, M.; Suda, H.; Mukaida, M.; Haraya, K.; Shimano, E.; Tsuji, T. Hydrogen Diffusion Coefficient and Mobility in Palladium as a Function of Equilibrium Pressure Evaluated by Permeation Measurement. *J. Membr. Sci.* **2012**, *421*−*422*, 355−360.
(29) Langhammer, C.; Zhdanov, V. P.; Zorić, I.; Kasemo, B. Size-Dependent Kinetics of Hydriding and Dehydriding of Pd Nanoparticles. *Phys. Rev. Lett.* **2010**, *104*, 135502−135506.
(30) Srivastava, V.; Balasubramaniam, R. Theoretical Modeling of Metal−Hydrogen Interactions in Pd Clusters. *Mat. Sci. Eng.: A* **2001**, *304*−*306*, 897−900.
(31) Eastman, J. A.; Thompson, L. J.; Kestel, B. J. Narrowing of the Palladium-Hydrogen Miscibility Gap in Nanocrystalline Palladium. *Phys. Rev. B* **1993**, *48*, 84−92.
(32) Lopez, N.; Łodziana, Z.; Illas, F.; Salmeron, M. When Langmuir Is Too Simple: $H_2$ Dissociation on Pd(111) at High Coverage. *Phys. Rev. Lett.* **2004**, *93*, 146103.
(33) Wilke, S.; Hennig, D.; Löber, R.; Methfessel, M.; Scheffler, M. Ab Initio Study of Hydrogen Adsorption on Pd(100). *Surf. Sci.* **1994**, *307*−*309* (Part A), 76−81.
(34) Grönbeck, H.; Zhdanov, V. P. Effect of Lattice Strain on Hydrogen Diffusion in Pd: A Density Functional Theory Study. *Phys. Rev. B* **2011**, *84*, 052301−052305.
(35) Johansson, M.; Skúlason, E.; Nielsen, G.; Murphy, S.; Nielsen, R. M.; Chorkendorff, I. Hydrogen Adsorption on Palladium and Palladium Hydride at 1 bar. *Surf. Sci.* **2010**, *604*, 718−729.
(36) Shabaev, A.; Papaconstantopoulos, D. A.; Mehl, M. J.; Bernstein, N. First-Principles Calculations and Tight-Binding Molecular Dynamics Simulations of the Palladium-Hydrogen System. *Phys. Rev. B* **2010**, *81*, 184103−184113.
(37) Sachs, C.; Pundt, A.; Kirchheim, R.; Winter, M.; Reetz, M. T.; Fritsch, D. Solubility of Hydrogen in Single-Sized Palladium Clusters. *Phys. Rev. B* **2001**, *64*, 075408−075418.
(38) Tanaka, K. Unsolved Problems in Catalysis. *Catal. Today* **2010**, *154*, 105−112.
(39) Pundt, A.; Suleiman, M.; Bähtz, C.; Reetz, M. T.; Kirchheim, R.; Jisrawi, N. M. Hydrogen and Pd-Clusters. *Mater. Sci. Eng.: B* **2004**, *108*, 19−23.
(40) Wilde, M.; Fukutani, K.; Naschitzki, M.; Freund, H. J. Hydrogen Absorption in Oxide-Supported Palladium Nanocrystals. *Phys. Rev. B* **2008**, *77*, 113412−113416.
(41) Mütschele, T.; Kirchheim, R. Segregation and Diffusion of Hydrogen in Grain Boundaries of Palladium. *Scr. Metall.* **1987**, *21*, 135−140.
(42) van Duin, A. C. T.; Dasgupta, S.; Lorant, F.; Goddard, W. A., III. ReaxFF: A Reactive Force Field for Hydrocarbons. *J. Phys. Chem. A* **2001**, *105*, 9396−9409.
(43) Senftle, T. P.; Meyer, R. J.; Janik, M. J.; van Duin, A. C. T. Development of a ReaxFF Potential for Pd/O and Application to Palladium Oxide Formation. *J. Chem. Phys.* **2013**, *139*, 044109−044115.
(44) Brenner, D. W. Empirical Potential for Hydrocarbons for Use in Simulating the Chemical Vapor Deposition of Diamond Films. *Phys. Rev. B* **1990**, *42*, 9458−9471.
(45) Tersoff, J. Empirical Interatomic Potential for Carbon, with Applications to Amorphous Carbon. *Phys. Rev. Lett.* **1988**, *61*, 2879−2882.
(46) Mortier, W. J.; Ghosh, S. K.; Shankar, S. Electronegativity-Equalization Method for the Calculation of Atomic Charges in Molecules. *J. Am. Chem. Soc.* **1986**, *108*, 4315−4320.
(47) Chenoweth, K.; van Duin, A. C. T.; Goddard, W. A. Reaxff Reactive Force Field for Molecular Dynamics Simulations of Hydrocarbon Oxidation. *J. Phys. Chem. A* **2008**, *112*, 1040−1053.
(48) Monti, S.; van Duin, A. C. T.; Kim, S. Y.; Barone, V. Exploration of the Conformational and Reactive Dynamics of Glycine and Diglycine on $TiO_2$: Computational Investigations in the Gas Phase and in Solution. *J. Phys. Chem. C* **2012**, *116*, 5141−5150.
(49) Quenneville, J.; Taylor, R. S.; van Duin, A. C. T. Reactive Molecular Dynamics Studies of DMMP Adsorption and Reactivity on Amorphous Silica Surfaces. *J. Phys. Chem. C* **2010**, *114*, 18894−18902.
(50) Raymand, D.; van Duin, A. C. T.; Spångberg, D.; Goddard, W. A., III; Hermansson, K. Water Adsorption on Stepped ZnO Surfaces from MD Simulation. *Surf. Sci.* **2010**, *604*, 741−752.
(51) Ludwig, J.; Vlachos, D. G.; van Duin, A. C. T.; Goddard, W. A. Dynamics of the Dissociation of Hydrogen on Stepped Platinum Surfaces Using the ReaxFF Reactive Force Field. *J. Phys. Chem. B* **2006**, *110*, 4274−4282.
(52) Zou, C.; Duin, A. T.; Sorescu, D. Theoretical Investigation of Hydrogen Adsorption and Dissociation on Iron and Iron Carbide Surfaces Using the ReaxFF Reactive Force Field Method. *Top. Catal.* **2012**, *55*, 391−401.
(53) van Duin, A. C. T.; Baas, J. M. A.; van de Graaf, B. Delft Molecular Mechanics: A New Approach to Hydrocarbon Force Fields. Inclusion of a Geometry-Dependent Charge Calculation. *J. Chem. Soc., Faraday Trans.* **1994**, *90*, 2881−2895.
(54) Wolf, R. J.; Lee, M. W.; Davis, R. C.; Fay, P. J.; Ray, J. R. Pressure-Composition Isotherms for Palladium Hydride. *Phys. Rev. B* **1993**, *48*, 12415−12418.
(55) Wolf, R. J.; Lee, M. W.; Ray, J. R. Pressure-Composition Isotherms for Nanocrystalline Palladium Hydride. *Phys. Rev. Lett.* **1994**, *73*, 557−560.
(56) Crespo, E. A.; Claramonte, S.; Ruda, M.; de Debiaggi, S. R. Thermodynamics of Hydrogen in Pd Nanoparticles. *Int. J. Hydrogen Energy* **2010**, *35*, 6037−6041.
(57) Ruda, M.; Crespo, E. A.; Debiaggi, S. R. d. Atomistic Modeling of H Absorption in Pd Nanoparticles. *J. Alloys Compd.* **2010**, *495*, 471−475.
(58) Crespo, E. A.; Ruda, M.; Ramos de Debiaggi, S. Hydrogen Absorption in Ni and Pd: A Study Based on Atomistic Calculations. *Int. J. Hydrogen Energy* **2008**, *33*, 3561−3565.
(59) Metropolis, N.; Rosenbluth, A. W.; Rosenbluth, M. N.; Teller, A. H.; Teller, E. Equation of State Calculations by Fast Computing Machines. *J. Chem. Phys.* **1953**, *21*, 1087−1092.
(60) Frenkel, D.; Smit, B. *Understanding Molecular Simulation: From Algorithms to Applications*; Academic Press: San Diego, 2002.
(61) Chase, M. W. *National Institute of Science and Technology NIST-JANAF Thermochemical Tables*; American Institute of Physics for the National Institute of Standards and Technology: Washington, D.C., 1998.

(62) Kresse, G.; Furthmuller, J. Efficiency of Ab-Initio Total Energy Calculations for Metals and Semiconductors Using a Plane-Wave Basis Set. *Comput. Mater. Sci.* **1996**, *6*, 15−50.
(63) Kresse, G.; Furthmuller, J. Efficient Iterative Schemes for *Ab Initio* Total-Energy Calculations Using a Plane Wave Basis Set. *Phys. Rev. B* **1996**, *54*, 11169−11186.
(64) Perdew, J. P.; Chevary, J. A.; Vosko, S. H.; Jackson, K. A.; Pederson, M. R.; Singh, D. J.; Fiolhais, C. Atoms, Molecules, Solids, and Surfaces: Applications of the Generalized Gradient Approximation for Exchange and Correlation. *Phys. Rev. B* **1992**, *46*, 6671−6687.
(65) Kresse, G.; Joubert, D. From Ultrasoft Pseudopotentials to the Projector Augmented-Wave Method. *Phys. Rev. B* **1999**, *59*, 1758−1775.
(66) Monkhorst, H. J.; Pack, J. D. Special Points for Brillouin-Zone Integrations. *Phys. Rev. B* **1976**, *13*, 5188−5192.
(67) Henkelman, G.; Uberuaga, B. P.; Jonsson, H. A Climbing Image Nudged Elastic Band Method for Finding Saddle Points and Minimum Energy Paths. *J. Chem. Phys.* **2000**, *113*, 9901−9904.
(68) Lide, D. R.; *Handbook of Chemistry and Physics: A Ready Reference Book of Chemical and Physical Data*, 84th ed.; CRC Press: New York, 2004.
(69) Cox, D. M.; Fayet, P.; Brickman, R.; Hahn, M. Y.; Kaldor, A. Abnormally Large Deuterium Uptake on Small Transition Metal Clusters. *Catal. Lett.* **1990**, *4*, 271−278.
(70) Zhdanov, V. P.; Kasemo, B. Kinetics of the Formation of a New Phase in Nanoparticles. *Chem. Phys. Lett.* **2008**, *460*, 158−161.
(71) Matsumura, D.; Okajima, Y.; Nishihata, Y.; Mizuki, J. Fast and Real-Time Observation of Hydrogen Absorption Kinetics for Palladium Nanoparticles. *J. Alloys Compd.* **2011**, *509*, S849−S852.
(72) He, J. H.; Knies, D. L.; Hubler, G. K.; Grabowski, K. S.; Tonucci, R. J.; Dechiaro, L. F. Hydrogen Segregation and Lattice Reorientation in Palladium Hydride Nanowires. *Appl. Phys. Lett.* **2012**, *101*, 153103.
(73) Holleck, G. L. Diffusion and Solubility of Hydrogen in Palladium and Palladium−Silver Alloys. *J. Phys. Chem.* **1970**, *74*, 503−511.
(74) Verlet, L. Computer "Experiments" on Classical Fluids. I. Thermodynamical Properties of Lennard-Jones Molecules. *Phys. Rev.* **1967**, *159*, 98−103.
(75) Berendsen, H. J. C.; Postma, J. P. M.; van Gunsteren, W. F.; DiNola, A.; Haak, J. R. Molecular Dynamics with Coupling to an External Bath. *J. Chem. Phys.* **1984**, *81*, 3684−3690.